

## Chapter 5

# Diffusion as Biology's Null Hypothesis for Dynamics

"The observations of which it is my object to give a summary in the following pages have all been made with a simple microscope." - Robert Brown, 1827

**Chapter Overview:** In which we consider the random motion of molecules

Dynamics in cells comes in a number of different forms. One of the most important classes of dynamical process is diffusion, the random jiggling of individual molecules in solution. When many such molecules are diffusing simultaneously, the overall concentration field undergoes changes in space and time that give the appearance of ordered and directed movements of molecules down concentration gradients. The goal of this chapter is to illustrate the important role of diffusion in living systems, a role we christen with the idea that it is biology's dynamical null hypothesis. As with many of the leading principles of science, there are many different ways to view and express our thinking on diffusion and here we compare and contrast microscopic and continuum, stochastic and deterministic, descriptions of diffusion. With the formalism in hand, we then turn to a suite of interesting biological questions that help illustrate the power of biology's null hypothesis for dynamics.

### 5.1 The Discovery of Brownian Motion

Biology is the study of complex interacting systems with many small parts that are constantly in motion and constantly undergoing change. We cannot even begin to think about biology without embracing concepts of motion and transformation. Even for sessile organisms such as plants, their cells are teeming with activity, as was already observed in the late 1700s by Bonaventura Corti with his discovery of what we now call cytoplasmic streaming and will discuss

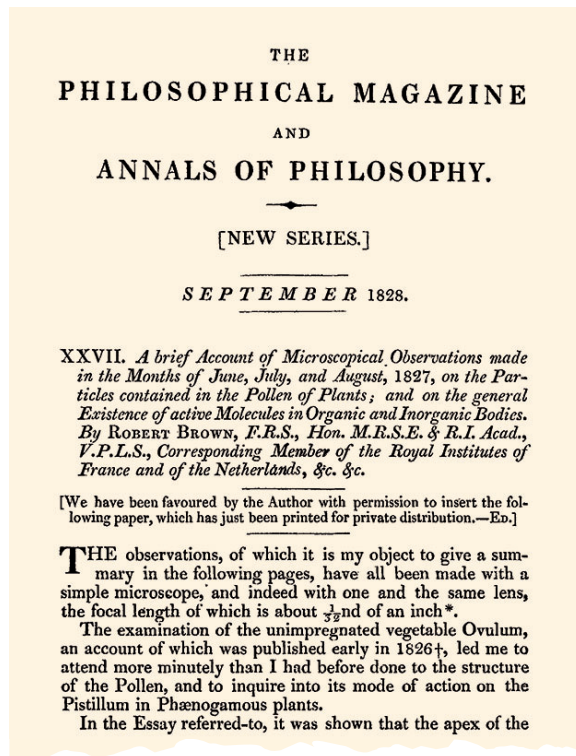


Figure 5.1: The announcement of the discovery of Brownian motion. The title of scientific papers in earlier times were charming, with Brown's great work signaling that random motions were common to inorganic and organic matter alike.

in more detail in later chapters. Half a century later, Robert Brown in his own investigations of plants and their pollen made the discovery of the fundamental motions that bear his name, announced in a paper with a wonderfully detailed title as shown in Figure 5.1.

The discovery of Brownian motion in the early 1800s led to generations of puzzlement and intellectual effort to understand what was going on, with Brown himself leading the way, positing at first that such motion was due to some sort of forces unique to living organisms. However, being the careful experimentalist that he was, he observed that such motion was present even in bizarre inorganic samples such as some dust from the famed Egyptian relic, the Sphinx. As we will see later in the chapter, the idea of the diffusion equation (and the heat equation) were already well in hand by this time. And yet, it wasn't at all clear how to reconcile the observations of discrete, punctuated motions as represented by Jean Perrin in Figure 5.2, and the familiar smooth diffusive profiles inherent in the solutions to the diffusion equation which tends to smooth heterogeneous

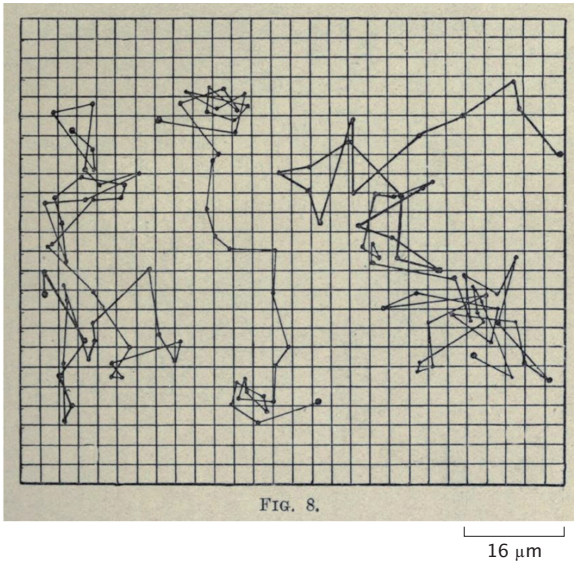


Figure 5.2: Direct observation of Brownian motion. These trajectories show data collected by Jean Perrin in 1913, observing the motion of small particles of the plant resin mastic (diameter about  $0.5 \mu\text{m}$ ). Each point represents the position of a particle recorded at 30 second intervals, and the lines indicate the net movement during that each interval. The side pf the grid squares is equivalent to  $3.2 \mu\text{m}$  (Adapted from Jean Perrin, *Les Atomes*, 1913.)

profiles. The merging of those two perspectives is one of the great success stories of modern science and will form the backdrop for the first half of our chapter.

## 5.2 The Mystery of Cellular Transport: Fast or Slow?

As we already saw in chap. 2, one of our principal aims is to develop what Barbara McClintock called “a feeling for the organism,” but often in the guise of a different question, namely, what sets the scale of X? Our claim is that by forcing ourselves to reflect on what sets the quantitative scale of a given problem, we sharpen our thinking about that problem and develop intuition for the knobs that control it. In this section, we ask two such questions in the context of diffusion with the ambition of developing intuition for diffusive time scales.

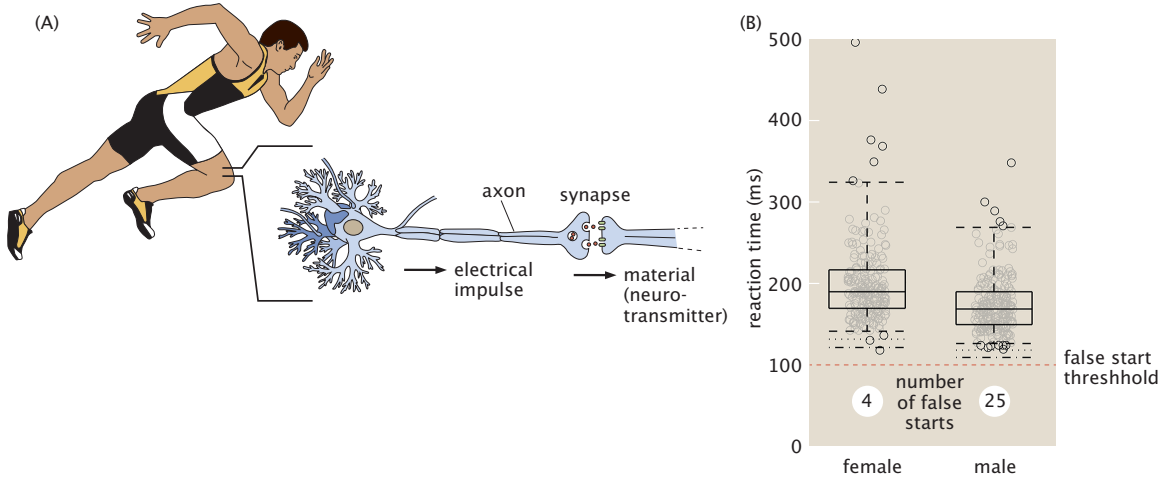


Figure 5.3: Human decision-making at the beginning of sprint races. (A) Sprinters leave their starting positions as a result of both electrical impulses along neurons and diffusion of neurotransmitters across the synaptic cleft. Together these processes determine reaction time. (B) Measured reaction times for sprinters from the olympics. The rules of international sprinting acknowledge the fact that no human can have a reaction time smaller than 100 ms.

### 5.2.1 The Puzzle of Sprinter Reaction Times

One of the most beautiful of human athletic spectacles is the 100 m dash, in which sprinters leave the starting blocks in a time less than 200 ms and less than 10 s later, are more than 100 m down the track. As shown in Figure 5.3, the reaction times of Olympic sprinters have been carefully measured revealing that for women and men alike, their reaction times are generally shorter than 200 ms. It is also interesting that international rules specify that by definition, if a sprinter leaves the starting block within 100 ms of the starting gun, it is a false start and leads to disqualification. The question we pose here is what sets the time scale of the reaction time?

From the moment the sprinter hears the firing of the starting gun until their foot leaves the block, a complex series of processes unfold throughout their body. We will ignore all but two of these processes. The argument we consider here asks about the relative speed of propagation of the action potential down the long nerves running from the brain to the feet and the diffusion time as the propagating signal is passed from one neuron to the next via synaptic diffusion. As seen in Figure 5.3, the synapse is the seat of material transport in the form of neurotransmitters across the roughly 30 nm gap separating adjacent neurons. To be precise, we wonder, which takes longer, for an action potential to travel 1 m along a neuron or for a neurotransmitter to diffuse across the synaptic gap?

### 5.2.2 Axonal Transport

A second related “what-sets-the-scale” question concerns the transport of amino acids within neurons. With the advent of radioactive tracers, pulse-chase experiments made it possible to follow the radioactivity, an approach that was the basis of Calvin’s classic papers on the “path of carbon in photosynthesis,” and also central to the study shown in Figure 5.4 that measured the transport of such radioactive amino acids in axons. As seen in the figure, radioactive leucine is injected in the neurons in the cell body and then the spatial distribution of that radioactivity is monitored during the following weeks. The question we ask here is whether the 16 day time scale for those radioactive amino acids to travel 30 mm is “long” or “short?” In the remainder of the chapter, we will develop the tools to give quantitative answers to the two diffusive transport questions posed in this section.

## 5.3 Diffusion in the Cell

Brownian motion is an inevitable outcome of the thermal jiggling of water molecules and does not indicate the activities of a living system. However, diffusive motion is always present at molecular length scales, and biological systems must tolerate, exploit, or inhibit Brownian motion in order to perform directed dynamic processes. A familiar example of the physical limits put on organisms by the process of diffusion is something you experience with every breath you take. Human metabolism demands a constant high concentration of oxygen supplied to mitochondria throughout the body. Much smaller organisms that are oxygen-dependent can rely simply on diffusion of oxygen as a delivery mechanism, but this is only efficient over distances of the order of tens of microns.

In order to grow to sizes exceeding 1 m, humans and other large animals have developed elaborate mechanisms to circulate oxygen and effectively enable its delivery to all tissues. In Chapter ??, we will examine hemoglobin as a protein specialized for the sole purpose of carrying oxygen to parts of the body far from the lungs. Oxygen inhaled in air can diffuse through lung tissue over an effective distance of roughly 100  $\mu\text{m}$  that is set not only by the free diffusion of oxygen, but also by its rate of consumption by cells in the tissue. In the lung, a fine network of capillaries surrounds each air sac and diffusion is sufficient for oxygen to travel from inhaled air to the hemoglobin-filled blood in the capillaries. Rapid fluid circulation, driven by your beating heart, carries the oxygen around the body much more rapidly than would be possible by simple diffusion. Reaching the tissues in the capillaries, oxygen molecules are again able to diffuse on a scale of 100  $\mu\text{m}$ . This sets the constant spacing of the finest branches of capillaries for all mammals from mice to blue whales.

In this chapter, we will make simple estimates about the distances over which passive transport (that is, diffusion) is effective and derive and apply the mathematical formalism of diffusion.

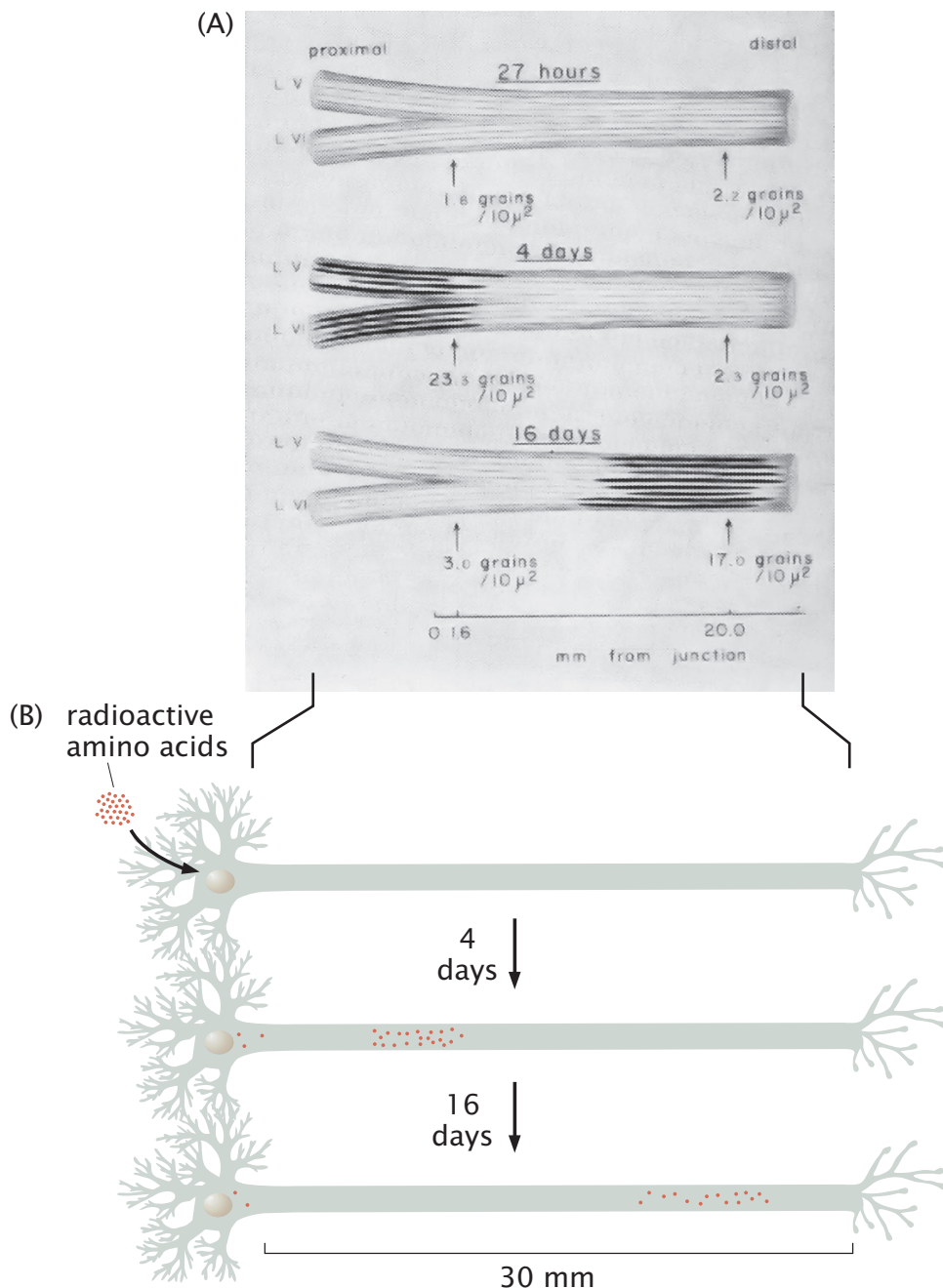


Figure 5.4: Transport of radioactively labeled amino acids in axons. (A) Experimental data from work from the early 1960s exploring transport of radioactively labeled leucine with a time scale of 16 days to travel  $\approx 30$  mm. (B) Schematic of the experiment and resulting data on axonal transport of radioactively labeled leucine.

### Diffusion Is the Random Motion of Microscopic Particles in Solution

Ions, molecules, macromolecular assemblies, and even organelles wander around aimlessly as a result of diffusion. Diffusion refers to the random motions suffered by microscopic particles in solution. As noted above, Brown noticed the random jiggling of pollen particles suspended in solution, even for systems that are ostensibly in equilibrium and have no energy source. Indeed, so determined was he to find out whether or not this was some effect intrinsic to living organisms, he even examined exotic suspensions using materials such as the dust from the Sphinx and found the jiggling there too. The effects of Brownian motion are palpable for particles in solution that are micron size and smaller, exactly the length scales that matter to cells. Diffusion results from the fact that in the cell (and for microscopic particles in solution), deterministic forces are on a nearly equal footing with thermal forces, an idea to be fleshed out in Section ?? (p. ??) and illustrated graphically in Figure 9.1 (p. 720). Thermal forces result from the random collisions between particles that can be attributed to the underlying jiggling of atoms and molecules. One of the simplest and far reaching ways we will develop a feeling for the numbers for these random motions is by introducing a critical energy scale associated with thermal motions and tied to the energy  $k_B T$ , where  $k_B$  is the Boltzmann constant.

**Estimate: The Thermal Energy Scale** One way to quantify the relative importance of the energy scale of a given process and thermal energies is by measuring the energy of interest in  $k_B T$  units. At room temperature, typical thermal energies are of the order of  $k_B T$ , with a value of

KEY EQUATION	
THERMAL ENERGY	
Boltzmann constant ( $1.38 \times 10^{-23} \text{ J/K}$ )	
$k_B T$	$\approx 4.1 \times 10^{-21} \text{ J} = 4.1 \text{ pN} \cdot \text{nm}$
temperature ( $\sim 300 \text{ K}$ )	natural energy scale of cells and their molecules

(5.1)

When the energy of a given process such as the removal of a charge from a protein is comparable to  $k_B T$ , barriers will be small (and probabilities of microstates high). The numerical value ( $k_B T \approx 4 \text{ pN nm}$ ) is especially telling since many of the key molecular motors relevant to biology act with piconewton forces over nanometer distances, implying a competition between deterministic and thermal forces. This discussion tells us that for many problems of biological interest, thermal forces are on a nearly equal footing with deterministic forces arising from specific force generation.

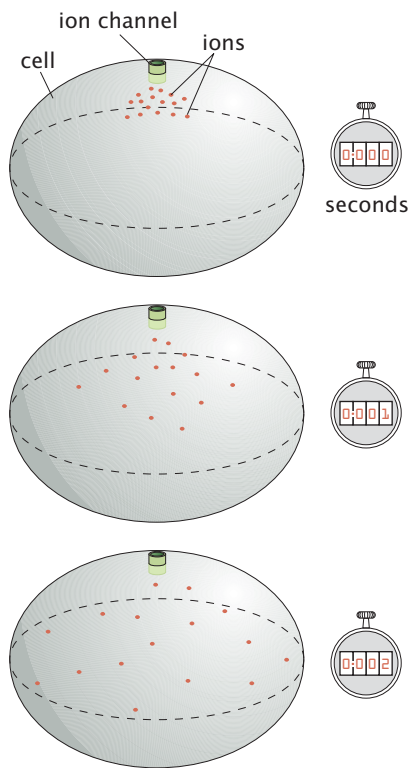


Figure 5.5: Schematic of the diffusion of ions just after opening of an ion channel. The three snapshots give a qualitative illustration of the distribution of ions as a function of time.

### 5.3.1 Active versus Passive Transport

The cell is teeming with motion. One of the first questions that one might ask about all of this bustling is to what extent it is random and to what extent active and directed. As will be discussed in detail in Chapter 9, the interplay between thermal and deterministic forces is one of the hallmarks of cellular dynamics. On the thermal side of the ledger, one of the dominant effects of the thermal forces is the very existence of diffusive motion itself. An example of the diffusion of various ion species after the opening of an ion channel is shown in Figure 5.5.

A second example that compares diffusive motion with directed motion is shown in Figure 5.6. In the top panel, we see a macromolecule subject to the thermic whims of its environment, every instant moving off in some new direction. By way of contrast, in the bottom panel, we see dynamics as mediated by active transport, such as through molecular motor driven cargo transport. In the pages that follow, we will be interested in learning how to distinguish these two modes of transport and how to compare them, a question that will lead us once again to the idea of dimensionless ratios already introduced in chap. 2,

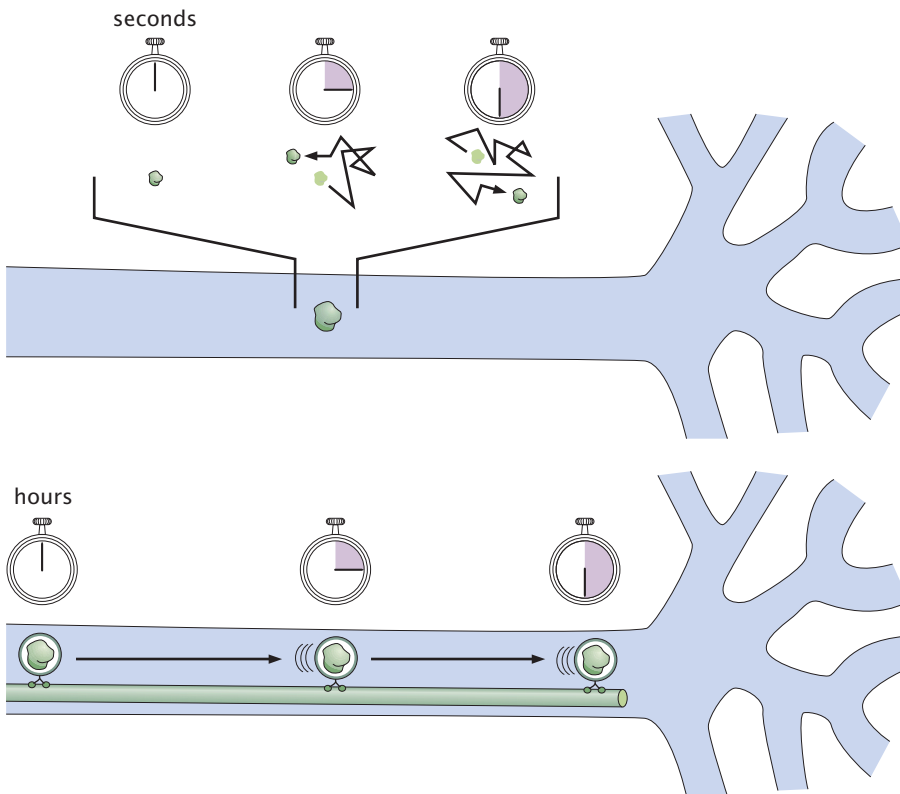


Figure 5.6: Transport within a nerve cell. (A) Passive transport of a molecule by diffusion. (B) Active transport of a molecule through directed motion of a molecular motor. **JT:** We need a third panel that shows the action potential.

this time resulting in the dimensionless Péclet number (see section 5.7.3, p. 340) that characterizes the relative importance of diffusive and active transport.

One of the most important results in all of physical biology is the simple formula that relates distance to diffusion time. That is, in order to understand the time scales of diffusive transport for processes such as those shown in Figures 5.5 and 5.6, we need to relate the length scale  $\ell$  over which diffusion occurs to the diffusion time  $t_{diff}$ . As we did in chap. 2, we begin by making very simple arguments using dimensional analysis to estimate diffusion times. To that end, Figure 5.7 shows how to make a simple scaling estimate for diffusion times. First, we hypothesize that the diffusion time depends upon two key parameters, the diffusion coefficient and the distance over which the diffusion takes place.

For the estimate in Figure 5.7 to actually make sense, we have to probe the meaning of the diffusion coefficient more deeply. Our first foray into the world of diffusive dynamics will be founded upon the idea of macroscopic concentrations

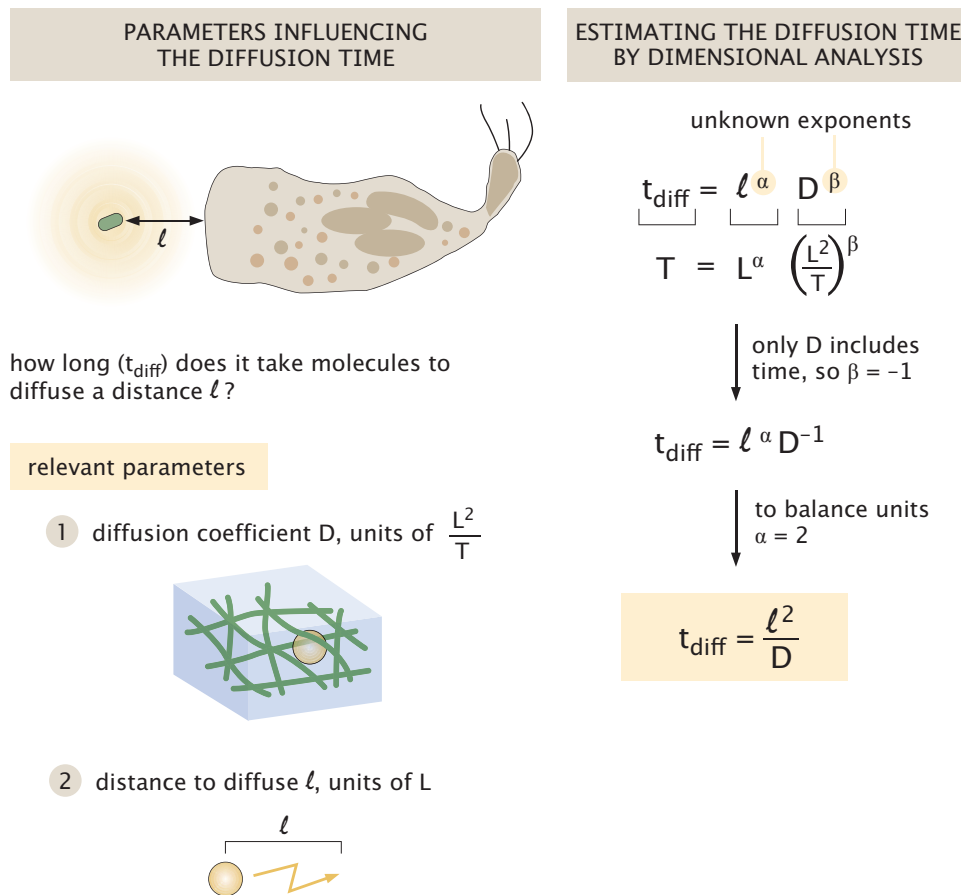


Figure 5.7: Using dimensional analysis to estimate the time scale for diffusion. In the left column, we posit that diffusion time depends upon two key physical parameters, the diffusion coefficient and the distance over which diffusion takes place. The right column shows how by balancing exponents we can find an expression for the diffusion time.

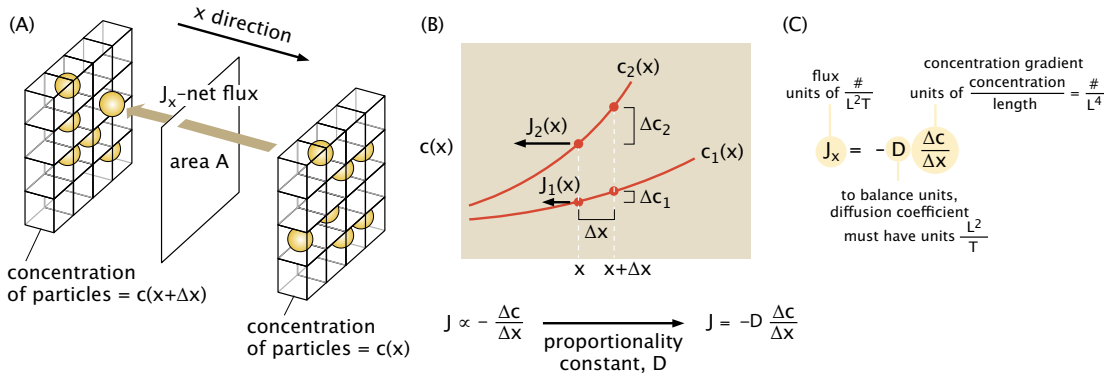


Figure 5.8: Relating the flux to the concentration through a constitutive model. Inferring Fick's law of diffusion, the constitutive equation of mass transport. What's the relationship between concentration,  $c(x)$ , and flux,  $J(x)$ ? (A) The net flux is given by the number of particles moving to the right minus the number moving to the left, divided by the area  $A$ . (B) Intuition tells us that a steep concentration gradient like  $c_2(x)$  will give rise to a large flux,  $J_2(x)$ . A shallower gradient,  $c_1(x)$ , will give rise to a smaller flux  $J_1(x)$ . Fick's law posits that flux is proportional to the slope (gradient) of the concentration as a function of position. (C) Noting the dimensions of all terms in Fick's law reinforces our understanding and reveals the units of the diffusion coefficient.

and fluxes as shown in Figure 5.8. Note that the concentration field tells us the average number of molecules per unit volume. More precisely, the concept is that we divide space up into a bunch of small boxes (such as shown in Figure 5.9), with the boxes large enough to include many molecules, but small enough so that the density is nearly uniform over the scale of the box. We use the notation  $c(\mathbf{r}, t)$  to signify the concentration in a box centered at position  $\mathbf{r}$  in three-dimensional space (with units of number of particles per unit volume) and  $c(x, t)$  to signify the concentration field in one-dimensional problems.

With the idea of a concentration in hand, we can consider the origins of diffusive dynamics. In particular, we begin by noting that in this macroscopic worldview, diffusive dynamics is the result of concentration gradients. What we mean precisely by the term “gradient” is a spatial variation in the concentration field. Figure 5.8(B) shows a simple concentration profile where on the right-hand side of the domain of interest, the concentration of the molecule of interest is high, while on the left-hand side of the domain of interest, the concentration is low.

The other key quantity of interest for our macroscopic description of diffusion is the flux. Flux can be thought of conceptually as shown in Figure 5.8(A), where it is seen that we identify a plane with some area  $A$  and then count the net number of molecules that cross that area per unit time. That is the

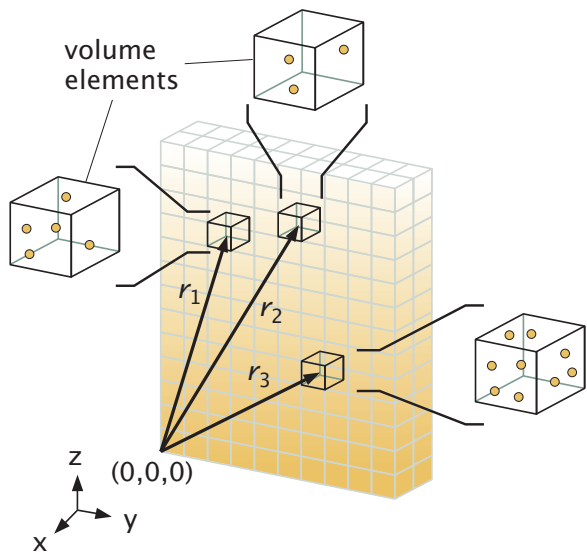


Figure 5.9: Defining the concentration field. The first step in the continuum theory protocol is the identification of the relevant field variables. For problems involving mass transport, the relevant field variable is the concentration field. For each material volume element, we count the number of molecules in that volume element and divide by the volume of that element. The concentration field can vary in both space and time.

component of the flux vector in that direction and corresponds to

$$\text{flux} = \frac{\text{number of particles}}{\text{area} \times \text{time}}. \quad (5.2)$$

In its full generality, the idea is more subtle than this, since in three dimensions, the flux is actually a vector whose components give the flux across planes that are perpendicular to the  $x$ -,  $y$ -, and  $z$ -directions. The goal of our thinking is to determine what amounts to an “equation of motion” that tells how the concentration field changes in both space and time.

### Fick's Law Tells Us How Mass Transport Currents Arise as a Result of Concentration Gradients

As a first cut, we treat this problem on strictly phenomenological grounds. Later in the chapter, we will show how this phenomenological law can be derived from microscopic considerations. For the time being, we restrict our attention to one-dimensional concentration profiles so that the resulting mathematics is simplified. Fick's first law is the assertion that the flux is linearly related to the concentration gradient, namely,

$$j = -D \frac{\partial c}{\partial x}, \quad (5.3)$$

where  $j$  which can be thought of as the number of particles crossing unit area per unit time and where  $D$  is the diffusion coefficient. (For a brief review of partial derivatives we refer the reader to The Math Behind the Models on p. 539.) The minus sign in Fick's law guarantees that the particle flux is in the right direction. For example, if we consider the profile shown in Figure 5.8(B), the concentration profile increases with increasing  $x$  ( $\partial c / \partial x > 0$ ). On the other hand, it is clear that molecules flow from the region of higher concentration to lower concentration, down the concentration gradient, in the negative  $x$ -direction. The units of  $D$  can be determined by examining the units of all of the other quantities in Fick's law. Note that it is conventional notation to characterize the units of a quantity  $D$  as  $[D]$  and the reader is asked to bear this in mind since the same notation is used to specify concentrations. Exploiting this scheme for Fick's law, we have The units of the right-hand side of the equation are

$$\left[ \frac{\partial c}{\partial x} \right] = \frac{\text{number of particles}/\text{length}^3}{\text{length}} = \frac{\text{number of particles}}{\text{length}^4}. \quad (5.4)$$

By rearranging our equation, we are left with the units of the diffusion coefficient, which are  $\text{length}^2/\text{time}$ . Note that the units of the diffusion coefficient are independent of the dimensionality of space. Typical values for the diffusion constant are shown in Table 5.10.

Now that we have an understanding of the dimensions of the diffusion coefficient, we can return to Figure 5.7. This figure shows that the typical time

molecule	measured context	diffusion coefficient ( $\mu\text{m}^2/\text{s}$ )	BNID
H <sub>2</sub> O	water	2000	104087, 106703
H <sub>2</sub> O	nucleus of chicken erythrocyte	200	104645
H <sup>+</sup> (from H <sub>3</sub> O <sup>+</sup> to H <sub>2</sub> O)	water	7000	106702
O <sub>2</sub>	water	2000	104440
CO <sub>2</sub>	water	2000	102625
tRNA ( $\approx$ 20 kDa)	water	100	107933, 107935
protein ( $\approx$ 30 kDa GFP)	water	100	100301
protein ( $\approx$ 30 kDa GFP)	eukaryotic cell (CHO) cytoplasm	30	101997
protein ( $\approx$ 30 kDa GFP)	rat liver mitochondria	30	100300
protein (NLS-EGFP)	cytoplasm of <i>D. melanogaster</i> embryo	20	109209
protein ( $\approx$ 30 kDa)	<i>E. coli</i> cytoplasm	7-8	100193, 107985
protein ( $\approx$ 40 kDa)	<i>E. coli</i> cytoplasm	2-4	107985
protein ( $\approx$ 70-250 kDa)	<i>E. coli</i> cytoplasm	0.4-2	107985
protein ( $\approx$ 140 kDa Tar-YFP)	<i>E. coli</i> membrane	0.2	107985
protein ( $\approx$ 70 kDa LacY-YFP)	<i>E. coli</i> membrane	0.03	107985
fluorescent dye (carboxy-fluorescein)	<i>A. thaliana</i> cell wall	30	105033
fluorescent dye (carboxy-fluorescein)	<i>A. thaliana</i> mature root epidermis	3	105034
transcription factor (LacI)	movement along DNA (1D, <i>in vitro</i> )	0.04 ( $4 \times 10^5 \text{ bp}^2 \text{s}^{-1}$ )	102036
morphogen (bicoid-GFP)	cytoplasm of <i>D. melanogaster</i> embryo	7	109199
morphogen (wingless)	wing imaginal disk of <i>D. melanogaster</i>	0.05	101072
mRNA	HeLa nucleus	0.03-0.10	107613
mRNA	various localizations and sizes	0.005-1	110667
ribosome	<i>E. coli</i>	0.04	108596

Figure 5.10: Table of diffusion coefficients for different molecules.

it takes for a particle to diffuse a distance  $L$  is given by  $t \approx L^2/D$ , where  $D$  is the diffusion constant of the particle. The diffusion constant has units of length<sup>2</sup>/time, and it depends on the size of the particle, the temperature, and the viscosity of the surrounding fluid. We will discuss this in detail later in this chapter. For the moment, we examine the numerical consequences of this simple, but important result.

### The Time It Takes a Diffusing Molecule to Travel a Distance $L$ Grows as the Square of the Distance

Unlike in the case of ballistic motion with constant velocity, where the time to travel a distance  $L$  grows linearly with the length scale of interest, diffusive dynamics implies that the time scale grows quadratically with distance. This result provides an opportunity for intuition-building by converting distances into the corresponding diffusion time as shown in Figure 5.11. In this figure, we plot the diffusion time as a function of the distance for  $D = 100 \mu\text{m}^2/\text{s}$ , a characteristic diffusion coefficient for a typical globular protein in water at room temperature. Note that the time scale associated with diffusion over a distance  $L \approx 10^6 \mu\text{m}$  (1m) is  $10^{10} \text{ s}$  ( $\approx$ 300 years)! This should make it clear that transport in cells and organisms requires mechanisms other than diffusion.

### 5.3.2 Answer to the Usain Bolt Question

Now that we have obtained our simple scaling result for how diffusion times scale with diffusion distance, we can return to the question of the relative time scale of action potential propagation and diffusion across the synaptic cleft for

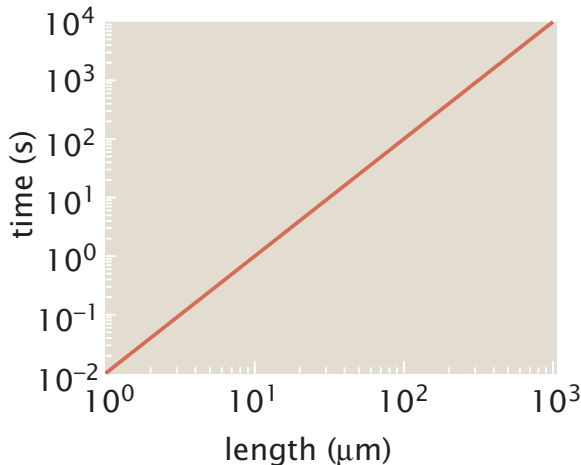


Figure 5.11: Diffusion time as a function of the length traveled for a typical value of the diffusion coefficient ( $D = 100 \mu\text{m}^2/\text{s}$ ) of a protein in water. The straight line on the log–log plot has a slope of 2 since time and distance are related by  $t = x^2/D$ .

sprinters on their starting blocks.

### Diffusive Transport at the Synaptic Junction Is the Dynamical Mechanism for Neuronal Communication

One of the classic episodes in the history of biology centered around the battle between Golgi, Ramon y Cajal, and their followers as to the nature of nerve transmission. At the heart of the controversy over soup versus sparks was the question of whether nerves are reticula (the view of Golgi) or rather built up of individual nerve cells, with communication between adjacent cells carried out by molecular transport. This debate was largely settled in favor of the “soup” view.

To estimate the time of propagation of the action potential, we use an action potential speed of  $f \times 10 \text{ m/s}$ , implying that the time for propagation along a 1 m neuron is

$$t_{ap} = \frac{L}{v} \approx \frac{1 \text{ m}}{f \times 10 \text{ m/s}} \approx \frac{f}{100} \text{ s}. \quad (5.5)$$

**Estimate: Diffusion at the Synaptic Cleft** The ideas introduced above can help us understand the dynamics of neurotransmitters at synapses. An example of the geometry of such a synapse is shown in Figure 5.12. Using exactly the same ideas as developed in the previous section, we can work out the time scale for neurotransmitters released at one side of the synapse to reach the receptors on the neighboring cell.

To be concrete, consider the diffusion of acetylcholine across a synaptic

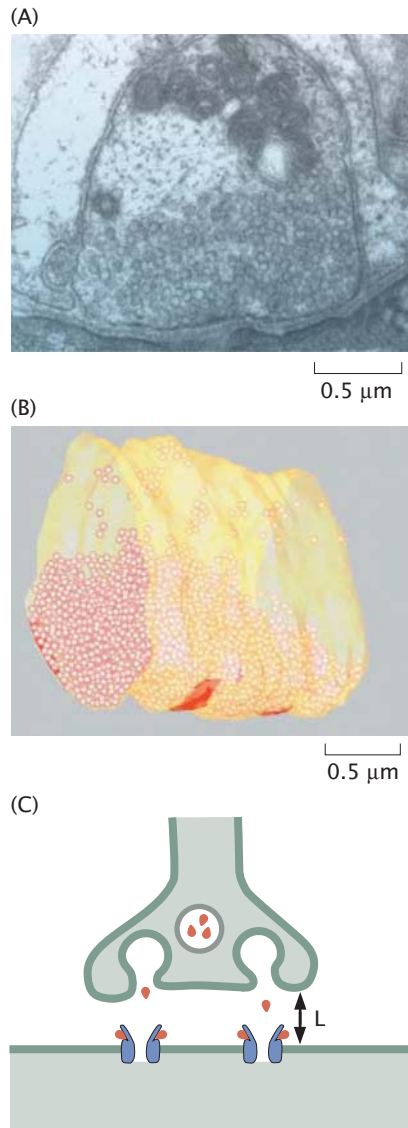


Figure 5.12: Geometry of the synapse. (A) Electron micrograph image of a nerve terminal. (B) Reconstruction of the synaptic geometry for a nerve terminal segment with a length of roughly  $2 \mu\text{m}$ . The many vesicles that are responsible for the active response of the synapse are shown in red. (C) Schematic of the diffusive transport across a synaptic cleft. (A and B, adapted from S. O. Rizzoli and W. J. Betz, *Nat. Rev. Neurosci.*, 6:57, 2005.)

cleft with a size of roughly 20 nm. Given a diffusion constant for acetylcholine of  $\approx 100 \text{ } \mu\text{m}^2/\text{s}$ , the time for these molecules to diffuse across the cleft is

$$t = L^2/D \approx \frac{400 \text{ nm}^2}{10^8 \text{ nm}^2/\text{s}} \approx 4 \text{ }\mu\text{s}. \quad (5.6)$$

### 5.3.3 Answer to the Question of Axonal Transport Times

#### Diffusion Is Not Effective Over Large Cellular Distances

The experiment described in Figure 5.4 inspires the question of whether the 16 days required for radioactive leucine to travel  $f$  mm is short or long. Of course, use of the words short and long beg the question: with respect to what time? Implicit in our question was an appeal to biology's null hypothesis for dynamics, namely, slow or fast with respect to how long it would take diffusion to transport those radioactive leucines by that distance. We can read off our answer to this question by extrapolating from the times shown in Figure 5.11 where we see that to travel 10s of mm, means that the leucine has traveled 10,000s of  $\mu\text{ms}$ , implying more than  $10^6 \text{ s}$ , a substantial part of the  $f \times 10^7 \text{ s}$  in a year. So our answer is that this time scale of 16 days is short with respect to diffusion.

The advent of high-resolution techniques for imaging living cells has touched all corners of biology. Beautiful radioactive labeling experiments like those shown in Figure 5.4 (p. 282) already made it clear that there is active transport within neurons, required because of the ineffective nature of diffusion over these long distances. More recently, single-cell microscopy has made it possible to watch axonal transport in real time as shown in Figure 5.13. In this case, quantum-dot labeled nerve growth factor (NGF) was tracked as it was transported in endosomes. Though there is cell-to-cell variability as seen in Figure 5.13(B), the mean transport rate of roughly  $1.3 \text{ }\mu\text{m/s}$  (see Figure 5.13(C)) leads to a much more reasonable transport time over a 1 cm neuron of  $10^4 \text{ s}$ , at least a two order-of-magnitude speed up relative to the time it would take diffusion to transport the molecules over the same distance.

Our thinking about the results of Figure 5.4 still remain incomplete. Specifically, although our appeal to diffusion led us to the conclusion that the transport was too fast relative to diffusion, the results from Figure 5.13 tell us that the leucine transport is too slow for simple ballistic transport at the speed of one motor. One possible explanation for this is given in Figure 5.14 where we see that in fact, such transport is intermittent, with periods of transport at fixed speed punctuated by episodes of pausing. This figure demonstrates the use of an analytical approach called a kymograph which is an efficient way of summarizing transport over both time and space. In this image, each vertical column of pixels represents a trace along the axon straightened out into a straight line. Moving from left to right, each column represents the same location at different times. Here the fluorescence images has been inverted so that the bright fluorescent protein shows up as a dark spot. Movement at a constant speed shows

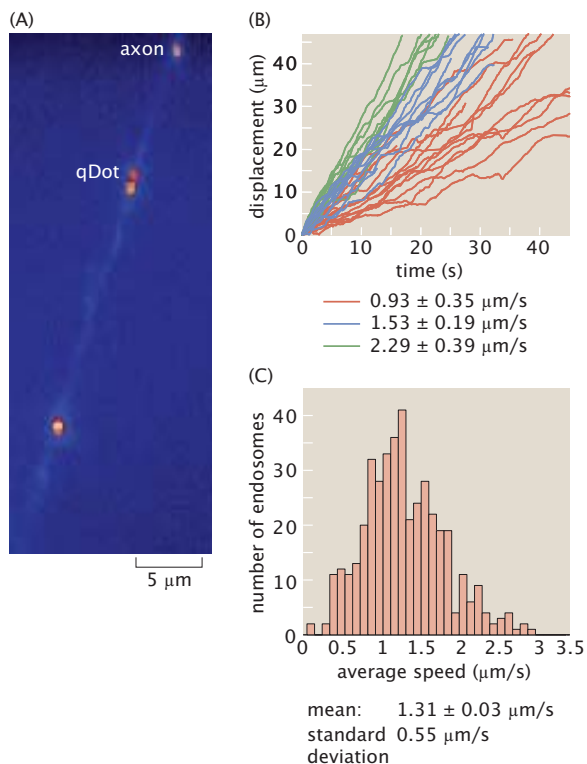


Figure 5.13: Transport in axons over short distances. (A) Quantum dots are used to label endosomes that are then tracked using fluorescence. (B) Endosomal transport in three separate neurons, each labeled by a different color. (C) Histogram of measured transport speeds. (Adapted from Cui2007)

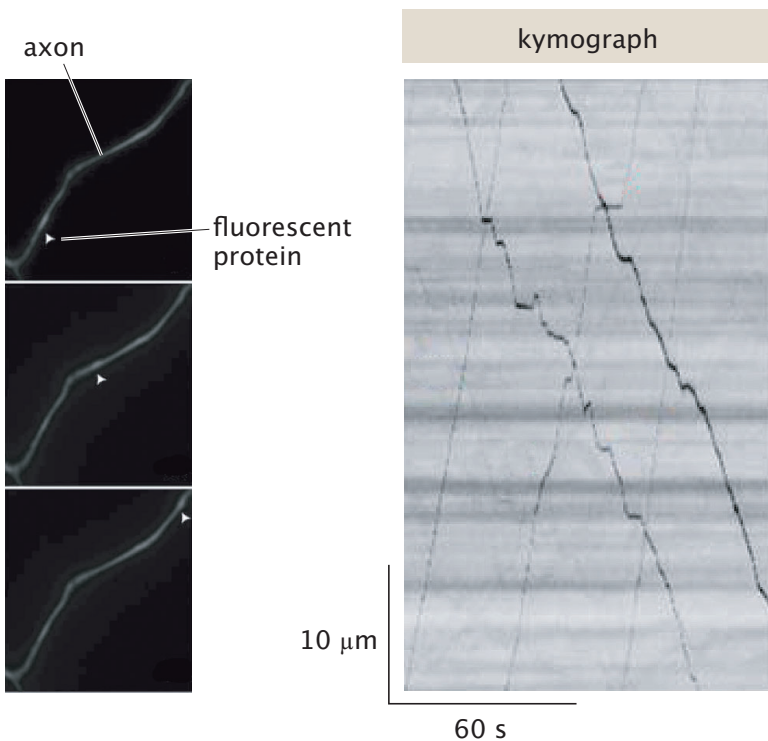


Figure 5.14: Protein transport along an axon. (A) Fluorescently labeled  $\alpha$ -synuclein particles are tracked as they are transported along the axon. (B) Kymograph of  $\alpha$ -synuclein particle movement revealing directed motion punctuated by pausing events. The rate of this transport is roughly  $2 \mu\text{m}/\text{s}$ . **RP:** HG reread to see where 2-8mm/day comes from (Adapted from Roy et al., J. Neurosci 28:5248 (2008))

up as a diagonal line, while periods of pausing appear as temporary horizontal interruptions. The analysis of this experiment in detail is left to the reader in the end of chapter problems.

*RP: work out time of transport with pauses for problems at end of chapter.*

### 5.3.4 A Random Walk Through Random Walks

The examples considered thus far in the chapter motivate the development of more formal theory to fully describe the diffusion process. In the upcoming sections we will explore three distinct concepts for exploring diffusion problems, each of which offers a unique view of random walks. Figure 5.15 provides a schematic overview of the upcoming sections.

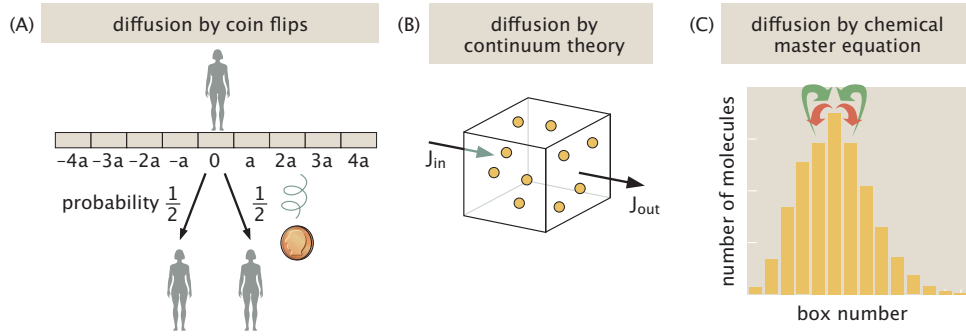


Figure 5.15: Three approaches to diffusion. (A) Diffusion as coin flips. (B) The continuum theory of diffusion. (C) Chemical master equation approach to diffusion.

## 5.4 Diffusion as Coin Flips

The first of the approaches considered in Figure 5.15 provides a stochastic analysis of the diffusion phenomenon, imagining that diffusive motions are produced by nothing more than random jiggling of all the constituent molecules through a random walk. Figure 5.16 introduces two views of such a random walker. In Figure 5.16(A) we imagine that our random walker starts out at the origin at time  $t = 0$ . At each time step, the walker flips a coin. If the coin comes up heads, the walker moves to the right (our right in the figure!). If the coin comes up tails, the walker moves to the left. A random walk trajectory is thus a collection of positions as shown in Figures 5.16(A) and 5.17. If we now imagine a huge number of walkers, all of whom start at the origin, then each one will generate its own trajectory as shown in Figure 5.18(A).

We can use the binomial distribution to determine averages, such as the position of the walker as a function of time. The walker's position for a given realization of the walk is

$$x = (n_h - n_t)a = (2n_h - N)a, \quad (5.7)$$

where in the latter step, we used the constraint that  $n_h + n_t = N$ . This means that the average position is given by

$$\langle x \rangle = (2\langle n_h \rangle - N)a. \quad (5.8)$$

We can evaluate  $\langle n_h \rangle$  using the binomial distribution by invoking the definition of the average as

$$\langle n_h \rangle = \sum_{n_h=0}^N n_h p(n_h, N) = \sum_{n_h=0}^N n_h \frac{N!}{n_h!(N-n_h)!} p^{n_h} q^{N-n_h}, \quad (5.9)$$

where, for mathematical convenience for the steps outlined below, we have defined  $q = 1 - p$  as the probability of making a step to the left. To make progress,

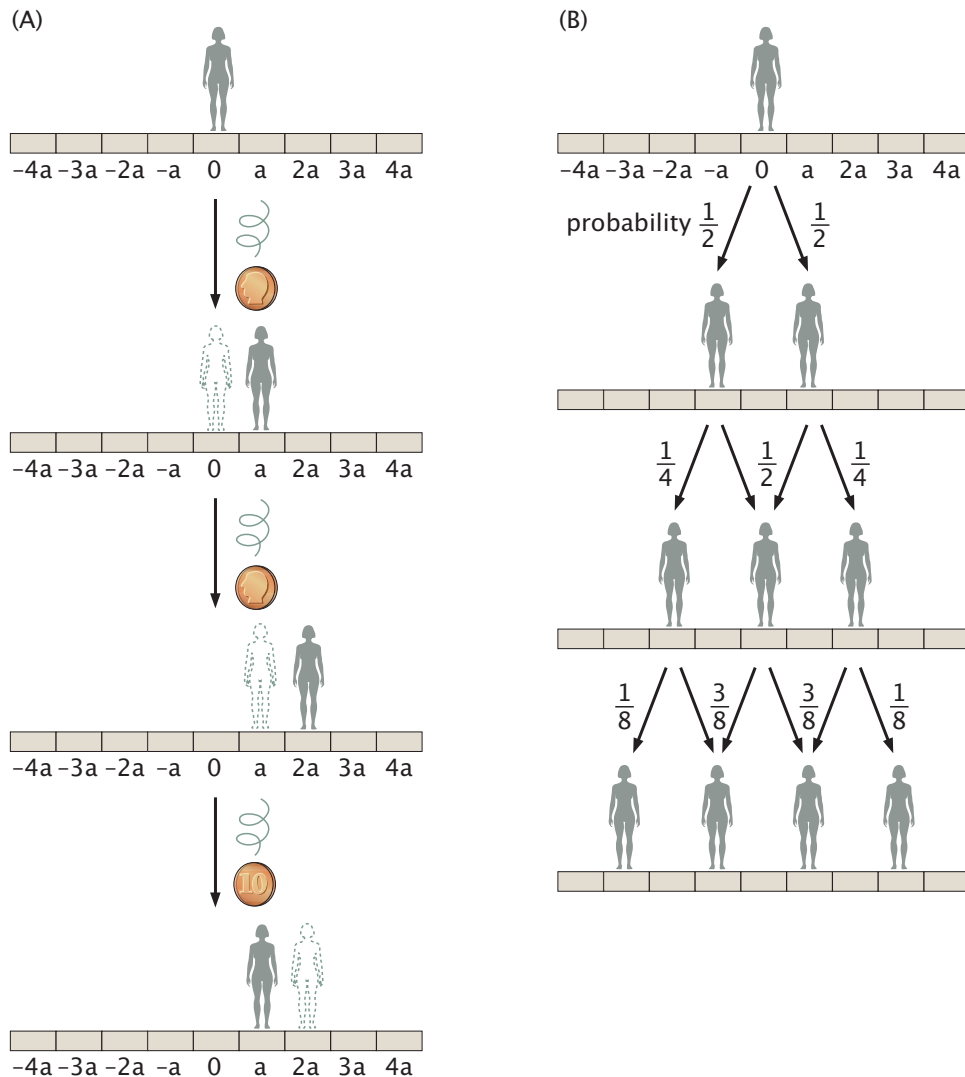


Figure 5.16: Coin flips and diffusion. (A) Stochastic “simulation” of a coin flipping process with the random walker stepping to the right when a heads is flipped and stepping to the left when a tails is flipped. (B) The binomial distribution tells the probability of each and every possible outcome after a total of  $N$  steps.

we appeal to the highly useful algorithm that we will use for evaluating averages of all of the great probability distributions shown in Figure 4.26 and in general throughout the book. As a reminder of what we already did in Section 4.1.2 (p. 220), this trick consists in realizing that the expression for the average of the distribution in Equation 5.12 can be written as the derivative of the binomial distribution itself. Namely,

$$\sum_{n_h=0}^N n_h \frac{N!}{n_h!(N-n_h)!} p^{n_h} q^{N-n_h} = p \frac{\partial}{\partial p} \sum_{n_h=0}^N \frac{N!}{n_h!(N-n_h)!} p^{n_h} q^{N-n_h}. \quad (5.10)$$

By the binomial theorem, which is left for the reader to prove in the problems at the end of the chapter, we know that

$$\sum_{n_h=0}^N \frac{N!}{n_h!(N-n_h)!} p^{n_h} q^{N-n_h} = (p+q)^N. \quad (5.11)$$

Such that the average number of heads can be written as

$$\langle n_h \rangle = p \frac{\partial}{\partial p} (p+q)^N = pN(p+q)^{N-1}. \quad (5.12)$$

Now, since  $p+q=1$ , we get

$$\langle n_h \rangle = Np. \quad (5.13)$$

As we know intuitively, for an honest coin,  $p=1/2$  and hence  $\langle x \rangle = 0$ . Though the average position is always zero as already seen in Figure 5.18(C), clearly the width of the distribution gets wider over time. How do we measure that width? Statistically, the quantity we want is

$$\langle (x - \langle x \rangle)^2 \rangle = \langle x^2 \rangle - \langle x \rangle^2, \quad (5.14)$$

which is also known as the standard deviation.

To make progress on evaluating this expression explicitly we now use the fact that

$$\langle x^2 \rangle = \langle (2n_h - N)^2 \rangle a^2 = (4\langle n_h^2 \rangle - 4\langle n_h \rangle + N^2)a^2. \quad (5.15)$$

To get our result, we thus need to compute  $\langle n_h^2 \rangle$  which can be done by appealing, once again, to the algorithm consisting of taking the derivative with respect to  $p$  as a way to bring  $n_h$  terms down from the exponent in the distribution. In this case, because we need to have  $n_h^2$  in the sum, we will take two such derivatives such that

$$\langle n_h^2 \rangle = \sum_{n_h=0}^N \frac{N!}{n_h!(N-n_h)!} n_h^2 p^{n_h} q^{N-n_h} = p \frac{\partial}{\partial p} p \frac{\partial}{\partial p} \sum_{n_h=0}^N \frac{N!}{n_h!(N-n_h)!} p^{n_h} q^{N-n_h}. \quad (5.16)$$

Once again, we invoke the binomial theorem which makes it possible to rewrite our results as

$$\langle n_h^2 \rangle = p \frac{\partial}{\partial p} p \frac{\partial}{\partial p} (p+q)^N = pN + p^2 N(N-1). \quad (5.17)$$

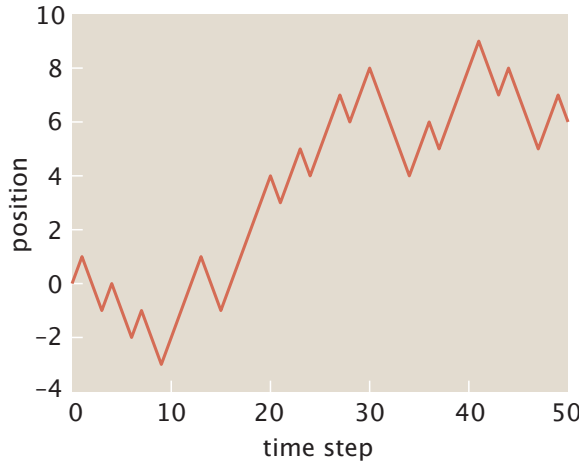


Figure 5.17: Position of a single walker diffusing by coin flips. At each time step, the random walker flips an honest coin and moves either left or right. The graph shows the position as a function of time.

We can now use our knowledge of  $\langle x \rangle$  as

$$\langle x \rangle = \langle 2n_h - N \rangle a = (2\langle n_h \rangle - N)a = (2Np - N)a. \quad (5.18)$$

Merging these results thus yields

$$\langle x^2 \rangle - \langle x \rangle^2 = 4Np(1-p)a^2. \quad (5.19)$$

How do we bring this mathematical description of coin flips back into contact with experimental studies of diffusion? We claimed that the molecules that exercise the random jiggling we know of as Brownian motion are engaged in precisely such a coin flipping game in the sense that they jiggle around aimlessly, with each step different from the previous (though note that generally we would have to consider walks in all three spatial dimensions). As a result, we can now begin to ask statistical questions about the distribution of positions the random walkers can be found in. For example, how wide is the distribution as a function of time? Figure 5.18(D) that results from averaging over many such coin flipping trajectories gives us the answer to that question where we see that the mean-squared displacement is given by

$$\langle x^2 \rangle \propto t. \quad (5.20)$$

What we see is that the width grows as the square root of the total number of steps taken. We can square this with our binomial distribution analysis by noting that the number of steps is given by  $N = t/\Delta t$ , and hence the mean-squared displacement from eqn. 5.19 can be written as

$$\langle x^2 \rangle = \frac{a^2}{\Delta t}t, \quad (5.21)$$

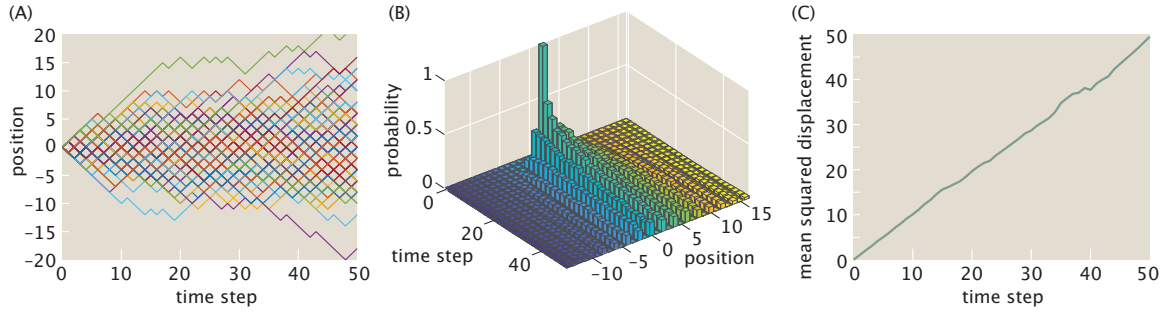


Figure 5.18: Statistics of diffusion by coin flips. (A) Trajectories of individual random walkers resulting from 100 simulations of diffusion by coin flips. (B) Distribution of positions of the walkers after each has taken the same number of steps. (C) Average position of the random walker as a function of time. (D) Mean squared displacement (square of the width of the distribution) as a function of the number of steps the walkers have made. **HG: Need to add C here**

with  $a^2/\Delta t$  serving as the diffusion coefficient. We invite the reader to explore diffusion by coin flips in the “Computational Exploration” below.

**Computational Exploration: Diffusion by Coin Flips** We can explore the distributions that arise from coin flips by recourse to a computer by using a random number generator to flip coins. In this computational exploration, the goal is to generate random walk trajectories like those indicated in Figure 5.16(A). A random walk trajectory is a series of positions on a one-dimensional lattice, with each successive position the result of either a left step or a right step from the previous position. Thus, the central idea is that the position at time step  $n$  is given by

$$x_n = x_{n-1} \pm a, \quad (5.22)$$

where  $a$  is the separation of lattice sites in the random walk. This already has the provocative form of a loop structure in a simulation with the key point being that at each step we have to decide whether to step left or right.

As mentioned above, in order to implement this stochastic decision, we will resort to a random number generator. Specifically, we will invoke a function that draws a random number between 0 and 1. As shown in Figure 5.19 we will divide this  $[0,1]$  segment in two parts: one corresponding to heads, and one corresponding to tails. In the case of a fair coin, the partition would be placed at 0.5 along this segment. We will continue using this trick for all our stochastic simulations throughout the book, where we will sometimes be dealing with unfair coins or more than two possible outcomes.

Using these tools, we can then loop over multiple random walkers. For each of these random walkers, we will loop through each time step. At each time step, we will flip the coin and keep track of the resulting position in

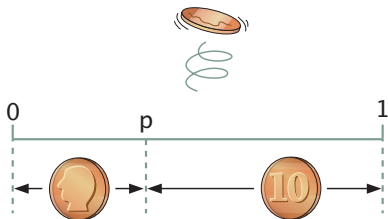


Figure 5.19: Using a random number generator to simulate coin flips. Simulating a dishonest coin flip, we generate a random number between zero and one. If that number is less than  $p$ , the outcome of that coin flip is a heads. Conversely, if that number is greater than  $p$ , the outcome of the coin flip is a tails. For  $p = 0.5$  we have a fair coin. **HG: Change it to an unfair coin using  $p$ ?**

order to generate trajectories such as those shown in Figure 5.18(A). Finally, once the trajectories for all walkers are obtained, we can generate histograms and quantify the random walk statistics as shown in Figures 5.18(B-D). These numerical results can then be compared to the predictions from the analytical solution to the random walk that are presented below.

The experimental data from Jean Perrin's classic book "Atoms" that opened this chapter (see Figure 5.2, p. 279) revealed the trajectories of Brownian particles when viewed in a microscope. These two-dimensional trajectories can be used to evaluate the mean-square displacement from which, in turn, we can infer the diffusion coefficient. Figure 5.20 shows this strategy in action for a simulation of 2D Brownian motion which builds on precisely the same coin-flipping ideas introduced above, but now with each walker faced with the prospect of moving in both the  $x$  and  $y$  directions. As we will see in subsequent sections, one of the primary ways of examining diffusive dynamics is by plotting the mean-squared displacement as a function of time as shown in Figure 5.21.

#### 5.4.1 Experimental Exploration of Diffusion in Living Systems

Thus far, our discussion of diffusion from the random-walker perspective has been abstract and mathematical. Can the ideas described above be directly parlayed into the analysis of experimental data from biological phenomena? In fact, the advent of the era of single-molecule biophysics has made it possible to watch individual molecules as they exercise random walks directly. Figure 5.22 gives a beautiful example involving the motion of the microtubule binding protein MCAK along microtubules. The conception of the experiment is very simple. Microtubules are labeled fluorescently with one color and the MCAK molecules are labeled a different color. Images are taken every 100 ms and the results of many such trajectories are assembled into a mean-square displacement curve as shown in Figure 5.22(C).

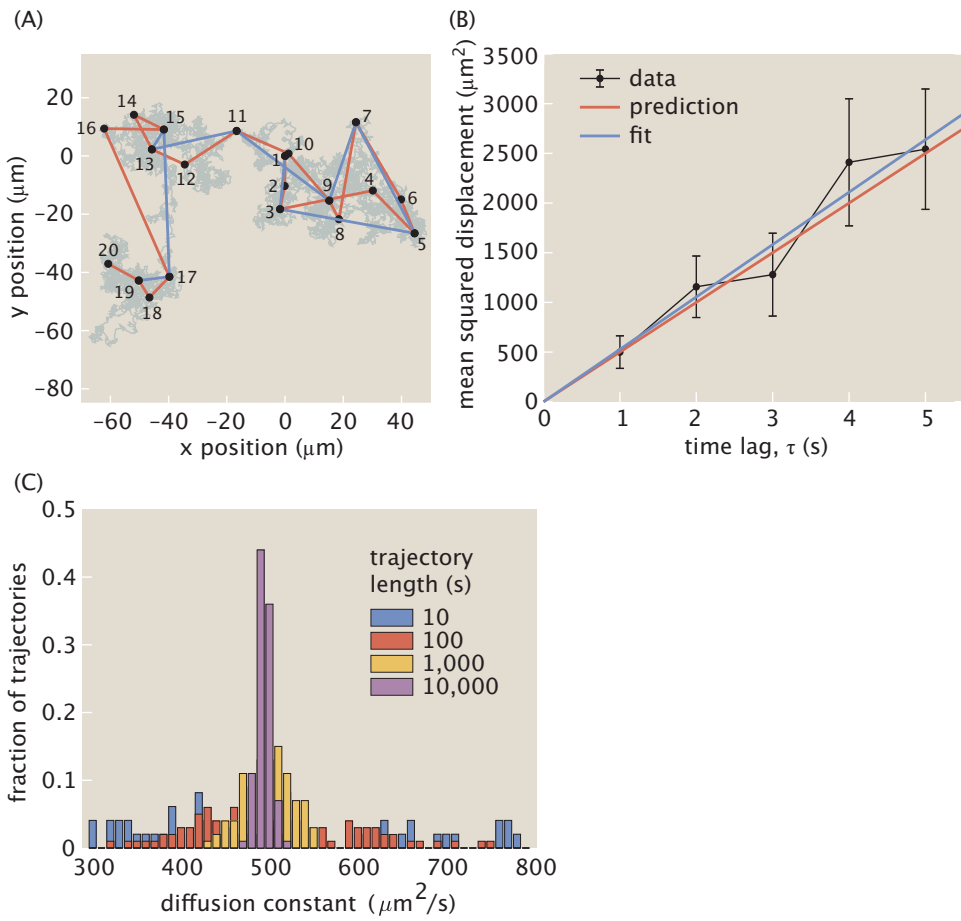


Figure 5.20: Brownian motion and inferring the diffusion constant. (A) Observed position of a Brownian particle as a function of time. (B) mean-square displacement and fit to data to obtain the diffusion constant. (C) Distribution of diffusion constants for different realizations of the diffusive dynamics. (A,B, Total trajectory time=20 s.  $D = 500 \mu\text{m}^2/\text{s}$ . Simulation time step=2 ms; C)

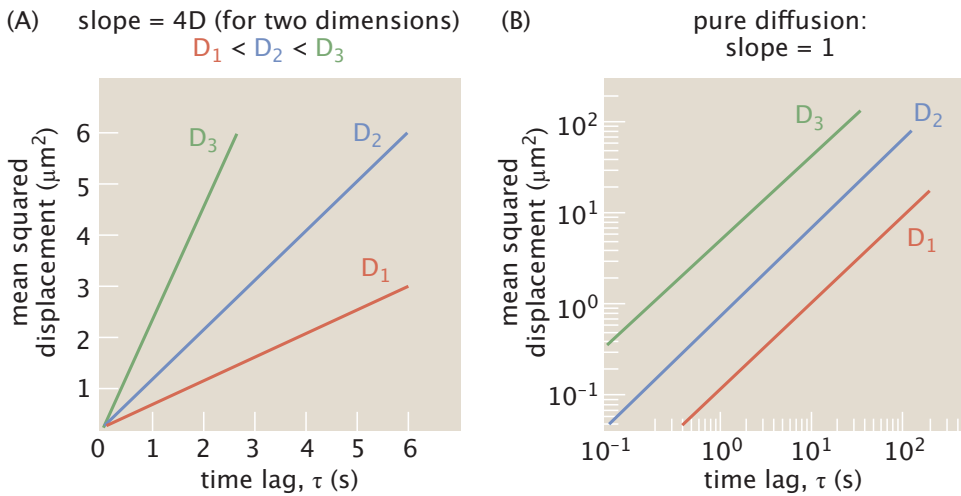


Figure 5.21: Comparison of linear and log-log plots for mean squared displacement. (A) For particles moving in two dimensions (such as proteins or lipids in a phospholipid bilayer),  $\text{MSD} = 4D\tau$ , so the slope of the line is equivalent to 4 times the diffusion coefficient. For particles moving with different diffusion coefficients, either because of differences in particle size, or because of differences in the viscosity of the medium, will produce lines with different slopes. (B) The same data shown on a log-log plot will always generate lines with a slope of 1 for particles undergoing a true random walk (pure diffusion). However, the vertical offset of the lines will vary depending on the diffusion coefficient.

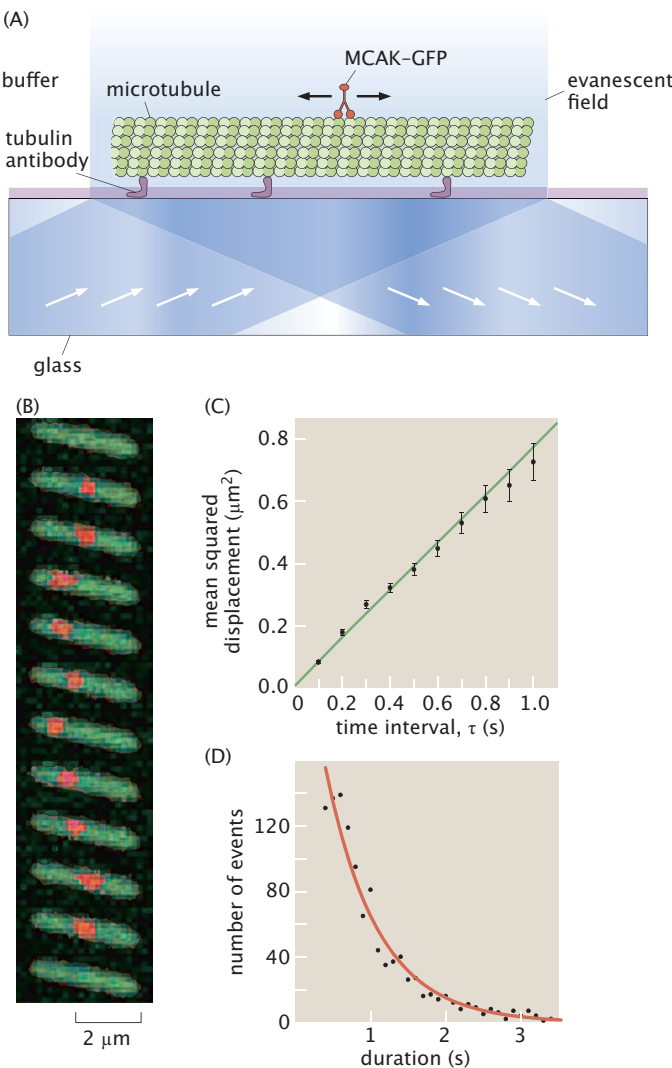


Figure 5.22: Direct observation of one-dimensional diffusion of a microtubule-binding protein. (A) Taxol-stabilized microtubules (green) are immobilized on a glass surface using anti-tubulin antibodies. The microtubule-binding protein MCAK (red) is labeled with a fluorophore such that single molecules can be visualized using evanescent wave microscopy. (B) In this series of images with one frame acquired every 100 ms, a single molecule of MCAK is observed to land on the microtubule and then move rapidly in both directions before dissociating. (C) The mean squared displacement for data pooled from over 1000 single molecule trajectories closely fits a straight line (green), indicating that the movement approximates one-dimensional diffusion with an apparent diffusion coefficient of about  $0.4 \mu\text{m}^2/\text{s}$ . (D) The interaction times of single MCAK molecules with microtubules closely follows an exponential distribution (red curve). (Adapted from Helenius et al., *Nature* 441: 115, 2006.)

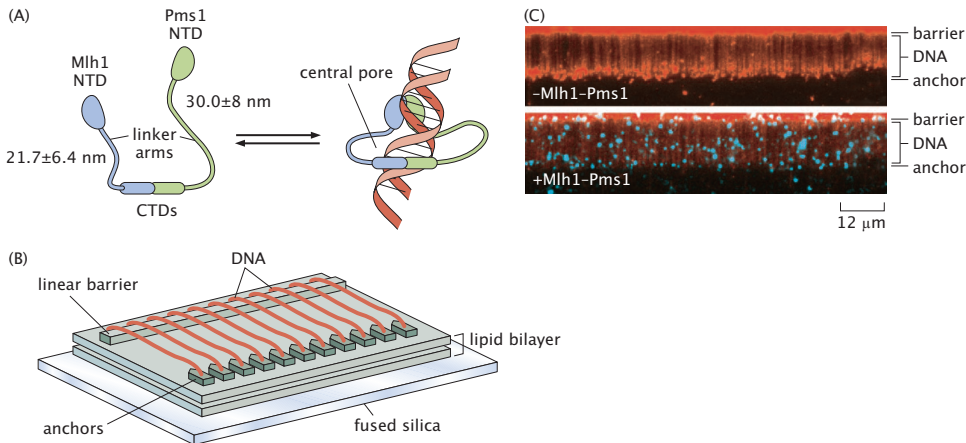


Figure 5.23: Direct observation of one-dimensional diffusion on DNA. (A) This schematic illustrates an experimental setup where many individual molecules of DNA with identical sequences can be arrayed into a “curtain,” where they all lie side by side. (B) The DNA is labeled red and individual DNA-binding protein complexes appear as blue spots. This particular protein complex has no sequence specificity so the blue spots can appear at any location along the DNA. **RP: remove part A**

A similar analysis to that described in Figure 5.22 for molecular motors on microtubules has been undertaken for the analysis of the motions of DNA-binding proteins on DNA as shown in Figure 5.23. Using a very clever technique known as DNA curtains, segments of DNA are stretched out to form a curtain of stretched one-dimensional DNA targets. As seen in the figure, when fluorescently labeled DNA binding proteins are added, their subsequent motion can be examined in the microscope and their mean-squared displacement analyzed. An even more sophisticated biological example is shown in Figure 5.24 using the same DNA curtain method. Here the idea is that the DNA is decorated with nucleosome complexes, a small disk-like object involving 8 histone proteins forming a protein octamer that is wrapped 1 3/4 times by roughly 150 bp of DNA. In the experiment shown here, it is seen that one of the protein complexes that binds the nucleosomal DNA is trapped between adjacent nucleosomes and thus is restricted to a confined random walk. By way of contrast, the Mlh1-Pms1 complex has the capacity to hop over nucleosomes to more broadly explore the DNA.

The *in vitro* experiments described above demonstrate that it is physically possible for a protein to undergo one-dimensional diffusion along a polymer such as a microtubule or DNA. However, these experiments were performed under unnatural conditions with vanishingly low protein concentrations and with salts and buffer that don’t reflect the intracellular milieu. This therefore raises the question of whether this kind of one-dimensional diffusion can take place in the

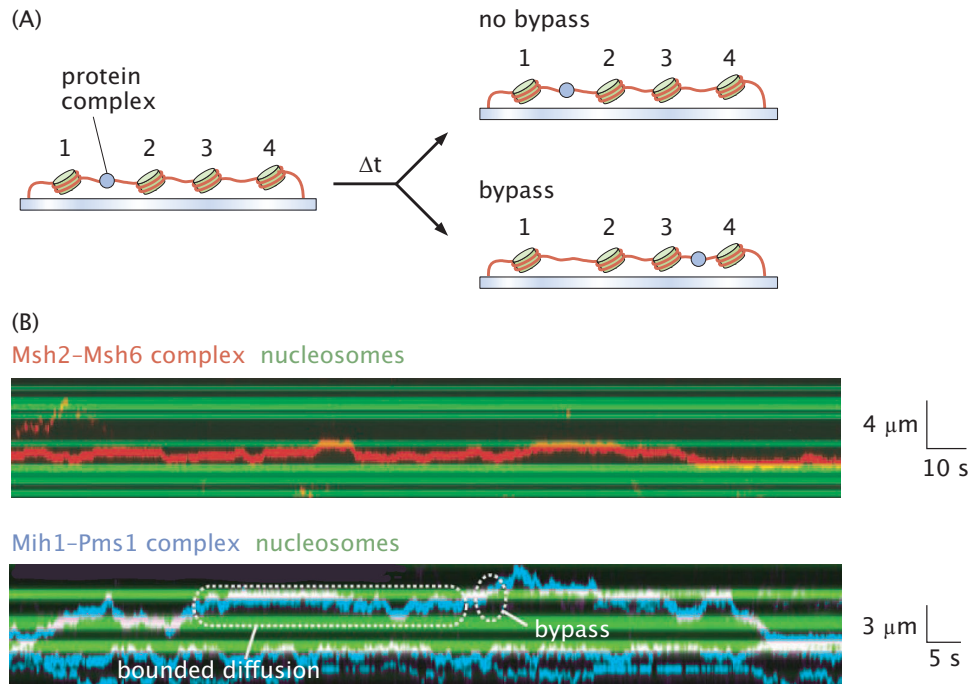


Figure 5.24: Use of DNA curtains to observe influence of nucleosomes on protein sliding along DNA. (A) The DNA curtain method illustrated in Figure 5.23 can be adapted by including nucleosomes that array themselves at specific locations. Individual protein complexes that find the nucleosome-free segments of DNA can be directly observed over time. (B) The Msh2-Msh6 complex slides along the free segments of DNA but cannot jump over the nucleosomes (shown in green), consequently the movement of one of these complexes appears as bounded one-dimensional diffusion between two neighboring nucleosomes. In contrast, the Mih1-Pms1 complex is able to hop over the nucleosome barriers so the traces illustrate stretches of time with bounded diffusion connected by discrete bypass events.

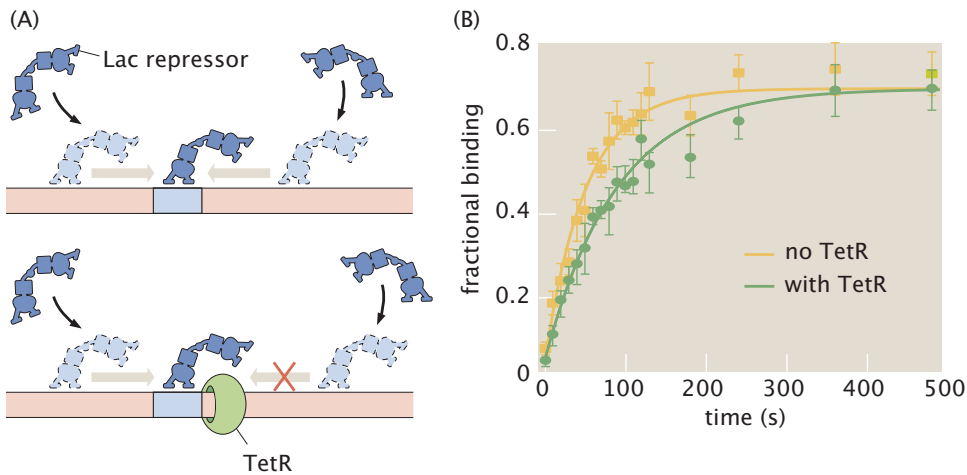


Figure 5.25: Experimental hints at the significance of one-dimensional diffusion in vivo. (A) Schematic of experimental setup showing the Lac repressor target site in blue and the use of the protein TetR as an obstacle. (B) Fractional binding as a function of time for the two constructs showed in part (A).

very different physical environment of a living cell. Figure 5.25 illustrates an experiment designed to test whether the presence of a blocking protein bound to a site on a bacterial chromosome can affect the kinetics of binding of a second protein to its target site. The model is that a sequence specific binding protein such as Lac repressor binds to its target site with high affinity, but also has some nonspecific affinity for any piece of DNA. In this scenario, Lac repressor molecules diffusing through the bacterial cytoplasm might arrive at the “wrong” site on the DNA and then slide using one-dimensional diffusion. If a roadblock is introduced on one side of the target binding site the net association of Lac repressor to its target site should be less efficient. The data shows a measurable although small effect.

So far in this section, we have seen how direct observations of positions of molecules over time can be analyzed to yield estimates for diffusion coefficients from in vitro experiments and also how implications of in vitro results can be used to formulate testable predictions for in vivo experiments. Of course, using modern microscopes and labelling methodologies, it is also possible to directly observe molecular mobility inside of living cells and measure quantitative aspects of molecular diffusion using the same approach that we have already explored. Figure 5.26 shows an impressive experiment where individual fluorescent molecules were tracked inside of living *E. coli* cells at a time interval of only 4 ms. These tracking experiments immediately reveal two striking findings. First, within the environment of a living cell, a small molecule moves much more quickly than a large complex such as a ribosome, with a scaling that approximately follows the Stokes-Einstein relation to be described later in the chapter.

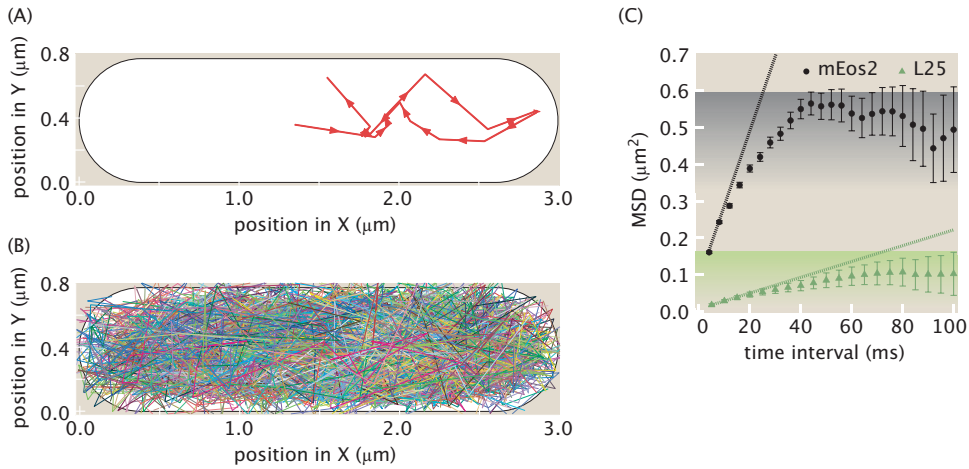


Figure 5.26: Single-particle tracking in living *E. coli* cells. (A) The trajectory of a single molecule of the photoactivatable protein mEos collected at 4 ms intervals from its initial activation until its death by bleaching. (B) Superimposed trajectories of over 1300 individual fluorophores tracked within a single cell. (C) Mean square displacement analysis for mEos (black symbols) and mEos attached to a ribosomal subunit (green symbols).

This approximate accord despite the fact that the physical environment inside of the cell is densely crowded and drastically different in many other ways from the dilute solutions for which that theory was initially developed. Second, although the expected diffusion model explains intracellular molecular motion well for short time scales (i.e., several ms), for these real tracks we can see that the mean square displacement quickly reaches a plateau. For a molecule inside a cell with a defined boundary, its mean-squared displacement can never go further than the distance from one side of the cell to the other. Therefore the position of the plateau in these experimental observations indicates the size of the cell.

## 5.5 The Continuum Theory Protocol

With the treatment of diffusion by coin flips behind us, we now turn to the second approach presented in Figure 5.15. For those with biological backgrounds, one of our hopes is to be able to introduce a few key theoretical protocols that will make it possible to attack a very broad array of problems. One of the most powerful of such protocols is the continuum theory protocol shown in Figure 5.27. As we will see throughout the book, this same protocol will serve us in hugely diverse applications ranging from the story of diffusion taken up here to the theory of elasticity that will help us understand the bending of DNA and membranes to the theory of hydrodynamics that will set the stage for thinking about swimmers as diverse as *E. coli* and the organisms that host it to the

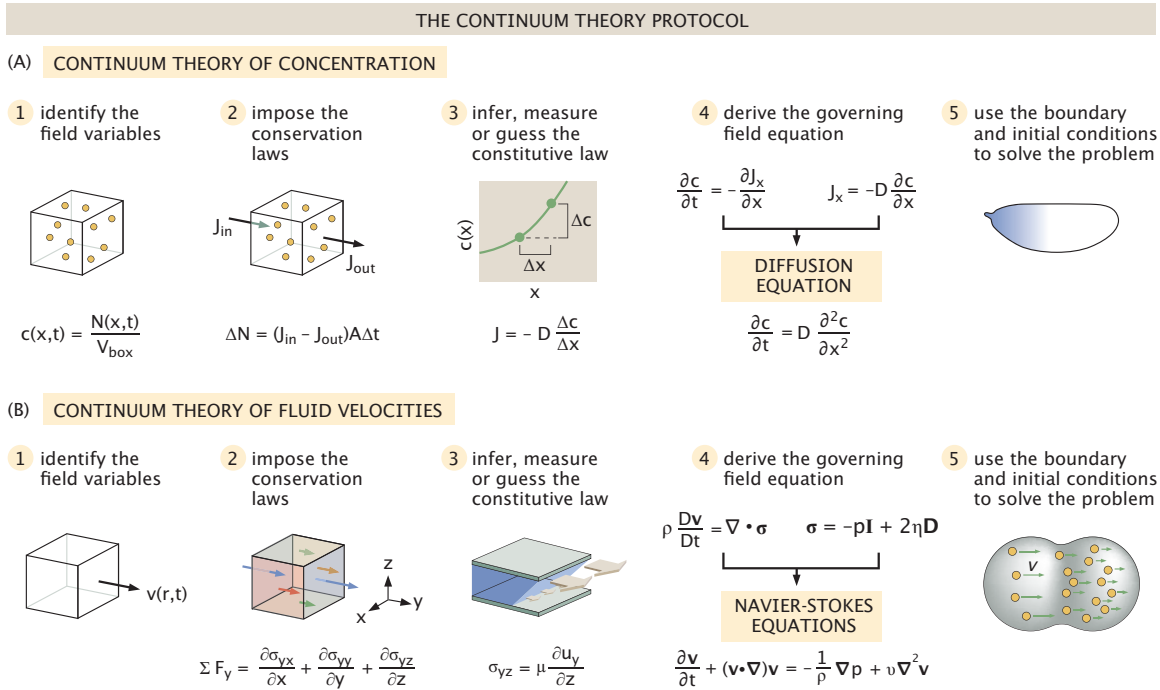


Figure 5.27: Continuum theory protocol. The top panel shows how to apply the continuum theory protocol to arrive at a continuum theory of diffusion. The bottom panel shows how the same protocol can be used to examine fluid motions as will be seen in Chapter 11.

exciting new area of the theory of active matter.

As seen in Figure 5.27, the continuum theory protocol has five essential steps. The first step in the protocol is essentially “kinematic” and amounts to figuring out what field variable we want to use to describe our system. Once we have determined the field variables, the next step is to impose the relevant conservation laws such as the conservation of mass or momentum. By itself, the conservation laws do not tell us how to relate the fluxes in the system to our field variables. For example, in the context of diffusion, we want to know how flux is related to the concentration. The third step in the continuum theory protocol is to find some way to relate fluxes to our underlying field variables. With these constitutive laws in hand, we turn to the fourth step which is to derive the relevant governing equation (usually a partial differential equation) that determines how our field variables evolve in space and time. With all of that hard work behind us in constructing the continuum theory for our system, the final step in the protocol is to solve the equations themselves to learn how our continuum evolves in space and time. We now examine each of those steps in more detail in the context of the important problem of diffusion which forms

the centerpiece of this chapter.

The first step in the continuum theory protocol as illustrated in Figure 5.9 is to establish the relevant field variables. Here we schematize our material system of interest as the classic continuum mechanics potato which is divided up into a collection of tiny cubes known as material volume elements. In each such material volume element, we define our field variable of interest. For example, in the context of the diffusion problem that is the central preoccupation of this chapter, the relevant field variable is the concentration field. This field is defined by visiting each material volume element whose address within the material is given by the position vector  $\mathbf{r}$  and to count up the number of molecules in that material volume element. In light of that accounting exercise, we then define the concentration as

$$c(\mathbf{r}, t) = \frac{N(\mathbf{r}, t)}{V}, \quad (5.23)$$

where  $N(\mathbf{r}, t)$  is the number of molecules in the material volume element at position  $\mathbf{r}$  and  $V$  is the volume of our tiny material volume element.

### The Diffusion Equation Results from Fick's Law and Conservation of Mass

With the concentration field in hand, we are now ready for the next step in the protocol which is to impose the relevant conservation laws. In this case, the conservation of mass can be written as an accounting statement about the box centered at point  $\mathbf{r}$ . For concreteness, consider the box shown in Figure 5.28, where we have specialized to the case in which the flux is only in the  $x$ -direction. This means that particles are flowing in and out on the two faces of the cube that are perpendicular to the  $x$ -direction. The basic strategy is to assess how many particles enter or leave at the face at position  $x - \Delta x/2$  and similarly across the face at position  $x + \Delta x/2$ . For the one-dimensional concentration gradient shown in Figure 5.28, the statement of conservation of mass can be written as

$$N(x, t + \Delta t) = N(x, t) + J(x - \frac{\Delta x}{2}, t) \Delta y \Delta z \Delta t - J(x + \frac{\Delta x}{2}, t) \Delta y \Delta z \Delta t. \quad (5.24)$$

This equation tells us that the number of particles in our little material volume element at time  $t + \Delta t$  is equal to the number in the box at time  $t$  plus all those particles that flowed in during the time increment  $\Delta t$  minus all of those particles that flowed out during that same time interval. We can rearrange the expression above by recalling that  $N(x, t + \Delta t) = c(x, t + \Delta t) \Delta x \Delta y \Delta z$  and by subtracting  $N(x, t)$  from both sides. Carrying out these steps, we are left with

$$\frac{c(x, t + \Delta t) - c(x, t)}{\Delta t} \Delta x \Delta y \Delta z = -[\frac{J(x + \frac{\Delta x}{2}, t) - J(x - \frac{\Delta x}{2}, t)}{\Delta x}] \Delta x \Delta y \Delta z. \quad (5.25)$$

We now recognize the terms on both sides as approximate expressions for derivatives. The left side gives the time derivative of the concentration and the right

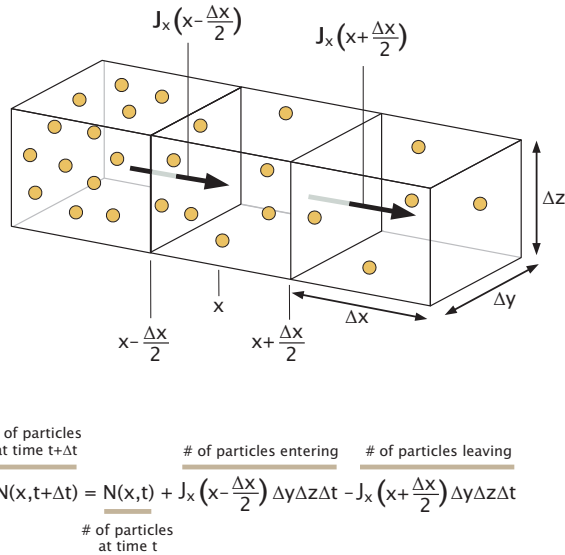


Figure 5.28: Imposing the conservation of mass. Conservation of mass implies that the change in the number of particles in a given material volume element in a small time interval  $\Delta t$  is equal to the number of particles entering minus the number of particles leaving.

side gives the spatial derivative of the flux. The net result is the so-called *local* form of the law of conservation of mass and can be written as

$$\frac{\partial c(x, t)}{\partial t} = -\frac{\partial J_x(x, t)}{\partial x}. \quad (5.26)$$

Note that this is a general statement about conservation of mass that transcends the particular details of any given system. If there are no chemical reactions that convert a molecule from one type to another or there are no production (i.e. transcription) or decay of molecules, then this conservation law must be respected. However, as stated, it is incomplete because we don't know how to relate flux  $J$  and concentration  $c$  and that brings us to the next step in the continuum theory protocol, namely, the elucidation of the constitutive model.

Often, the third step in the continuum theory protocol is where the “art” of modeling rears its head, asking us to infer, measure or even guess how the material responds. Unlike the absolute status of the law of conservation of mass, often, the material response embodied in our constitutive models is material specific and only applies over some limited regime of conditions in the material. For example, in the diffusion example considered here, we are going to work in a dilute limit where we assume that each and every diffusing particle acts independently. However, clearly there are regimes of concentration where the particles do not act independently and in that case, the law of material response (Fick's law) we will establish here would be superseded by some other form of

*RP: independence approximation - do an estimate*

material response.

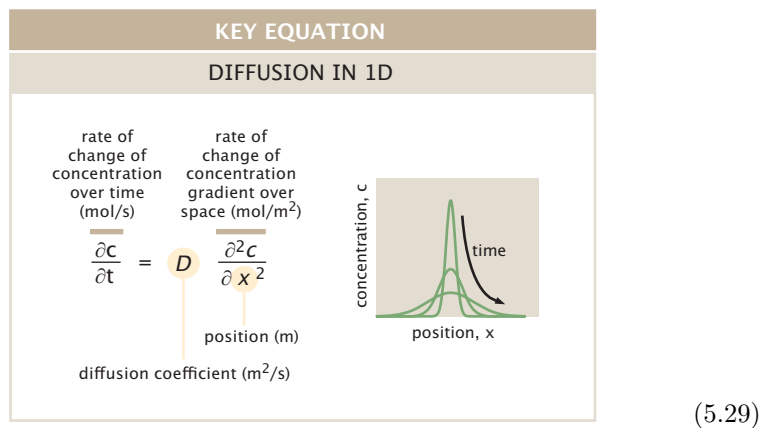
For the case of diffusion of interest here, Figure 5.8 asks us how to relate the concentration field variable  $c(x, t)$  to the flux field variable  $J_x(x, t)$ . As seen in part (A) of the figure, the net flux will be from the side with more particles to the side with less. As shown in part (B) of the figure, the flux will be larger, the greater the difference in the number of particles in the adjacent boxes. As we already saw in our discussion of the dimensions of the diffusion constant, the simplest formulation of a constitutive law for mass transport is Fick's law given by

$$J(x, t) = -D \frac{\partial c(x, t)}{\partial x}. \quad (5.27)$$

The next step in the continuum theory protocol is to link the conservation law and the constitutive law to establish the governing field equations for the continuum problem of interest. In the context of diffusion this means that we substitute our expression for the flux in terms of the concentration as embodied in eqn. 5.100 into the conservation law as given by eqn. 5.26 with the result that

$$\frac{\partial c(x, t)}{\partial t} = -\frac{\partial}{\partial x} \left( -D \frac{\partial c(x, t)}{\partial x} \right). \quad (5.28)$$

The outcome of this analysis is the famed diffusion equation given by



The final step in the continuum theory protocol of Figure 5.27 is to use the governing field equation(s) to solve some problem of interest as shown in Figure 5.29. As seen in the figure, to solve a given problem, we need to provide two kinds of information that describe it. As stated, governing equations such as the diffusion equation of eqn. 5.29 are very general. The same equation describes the dynamics of chemoattractants surrounding a pipette as the penetration of carbon atoms into a steel surface. As a result, there has to be some way to tell the governing equation what the particular details are that characterize our problem of interest. For a diffusion problem, this means stating the initial concentration field,  $c(x, 0)$ , which tells us how the concentration starts out at

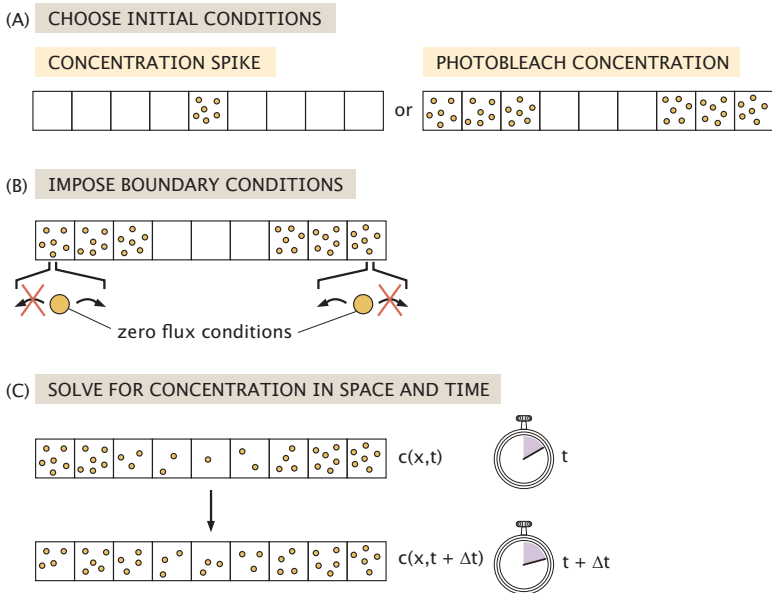


Figure 5.29: Imposing initial conditions and boundary values to use the continuum theory to solve specific problems. (A) Initialize the concentration field at time  $t = 0$ . (B) Impose the boundary conditions. In the schematic shown here, there is zero flux at the two boundaries. (C) Given the initial conditions and the boundary conditions, the change in the concentration can be evaluated by integrating forward in time.

time  $t = 0$ . The second key information that must be provided is the boundary conditions which tell us how the concentration or fluxes are treated on the boundary of our system.

### 5.5.1 Solutions and Properties of the Diffusion Equation

#### Concentration Profiles Broaden Over Time in a Very Precise Way

Now that we have the diffusion equation in hand, it is of great interest to examine its biological consequences. One of the most useful tools corresponds to knowing how to solve this equation for a spike of concentration at the origin at time  $t = 0$ . In particular, if at time  $t = 0$  we start with  $N$  molecules in an infinitesimally small region around  $x = 0$ , the concentration profile will evolve in the following way:

$$c(x, t) = \frac{N}{\sqrt{4\pi Dt}} e^{-x^2/4Dt}. \quad (5.30)$$

The solution itself is left to the problems at the end of the chapter. Further, by dividing by  $N$ , this equation can then be interpreted as giving the probability

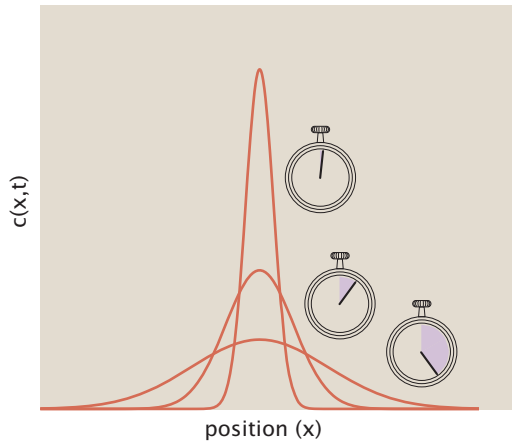


Figure 5.30: Time evolution of the concentration field. The plot shows the solution for the diffusion equation at different times for an *initial* concentration profile that is a spike at  $x = 0$ .

density for finding a particle between  $x$  and  $x+dx$ . The solution quoted above is often denoted as the Green's function of the diffusion equation and its evolution can be seen in Figure 5.30. This equation for the concentration tells us that the profile has the form of a Gaussian. The width of the Gaussian is  $\sqrt{2Dt}$  and hence it increases as the square root of the time. One of the most beautiful features of a solution like this is that once it is known, by exploiting the linearity of the diffusion equation itself, we are then free to write the solution for an arbitrary initial distribution of diffusing molecules. This idea will be taken up in the problems at the end of the chapter.

Note in Figure 5.30 that the mean position of the concentration distribution does not change with time. This corresponds to the absence of a drift term. On the other hand, even in the absence of drift, the diffusive dynamics is rich and interesting. One of the most interesting quantities to feature is the width of the distribution,  $\langle x^2 \rangle$ , which broadens over time. Since the distribution is Gaussian, we can essentially read off the dynamics of the width, but we take this opportunity to compute it explicitly since it is instructive both physically and mathematically. To compute this broadening, we need to evaluate  $\langle x^2 \rangle$  as

$$\langle x^2 \rangle = \frac{\int_{-\infty}^{+\infty} x^2 \frac{N}{\sqrt{4\pi Dt}} e^{-x^2/4Dt} dx}{N} = \frac{1}{\sqrt{4\pi Dt}} \int_{-\infty}^{+\infty} x^2 e^{-x^2/4Dt} dx, \quad (5.31)$$

where we have made use of the probability distribution for finding a particle at position  $x$  at time  $t$ , which is related to the concentration distribution, Equation 5.30, by  $c(x,t)/N$ . Using the trick introduced in The Tricks Behind the

Math below, we can evaluate this integral straightaway to find

$$\langle x^2 \rangle = \frac{1}{\sqrt{4\pi Dt}} \int_{-\infty}^{+\infty} x^2 e^{-x^2/4Dt} dx = \frac{1}{\sqrt{4\pi Dt}} \frac{\sqrt{\pi}}{2} (4Dt)^{3/2} = 2Dt. \quad (5.32)$$

Note that this is the key result that we have already invoked a number of times throughout the book as the basis of intuition about diffusive processes. In particular, this is the result that we have argued reveals how diffusion times scale with the square of the distance over which diffusion must act.

**The Tricks Behind the Math: Doing Integrals by Differentiating With Respect to a Parameter** Sometimes the knowledge of one integral in terms of a parameter appearing in the integrand can be used to compute a number of related integrals obtained by differentiating with respect to the parameter in question. In the case of the Gaussian integral,

$$\int_{-\infty}^{\infty} e^{-\alpha x^2} dx = \sqrt{\frac{\pi}{\alpha}}, \quad (5.33)$$

we can differentiate both sides of the equation with respect to the parameter  $\alpha$  to obtain

$$\int_{-\infty}^{+\infty} x^2 e^{-\alpha x^2} dx = -\frac{\partial}{\partial \alpha} \int_{-\infty}^{+\infty} e^{-\alpha x^2} dx = -\frac{\partial}{\partial \alpha} \sqrt{\frac{\pi}{\alpha}} = \frac{\sqrt{\pi}}{2\alpha^{3/2}}. \quad (5.34)$$

If we differentiate with respect to  $\alpha$  a second time, this yields  $\langle x^4 \rangle$ . Repeated differentiation with respect to  $\alpha$  allows us to determine all of the even moments.

### 5.5.2 FRAP and FCS

**Experiments Behind the Facts: Measuring Diffusive Dynamics** There are a number of different techniques that permit the investigation of diffusive dynamics within cells. Here, we consider three examples of some of the ingenious techniques that have been introduced to measure diffusion: FRAP, single-particle tracking, and fluorescence correlation spectroscopy (FCS).

FRAP takes advantage of the annoying feature of fluorescently labeled molecules that when they are exposed to too much light they no longer fluoresce, since the fluorophores can only emit a limited number of photons. In this instance, this weakness is turned into a strength by virtue of the fact that it can be used to measure diffusive dynamics within cells. The technique is illustrated schematically in Figure 5.31. In particular, a laser is focused on a certain spot in the cell with characteristic dimensions of a micron or larger. After the laser pulse, other fluorescently labeled molecules from elsewhere within the cell diffuse back into the space that had previously been photobleached by the laser light. By watching the time course of the recovery of fluorescence, it is possible to extract features of the diffusive dynamics.

An example of the appearance of cells during the FRAP experiment is shown in Figure 5.32. In the series of snapshots, the bleached region shows

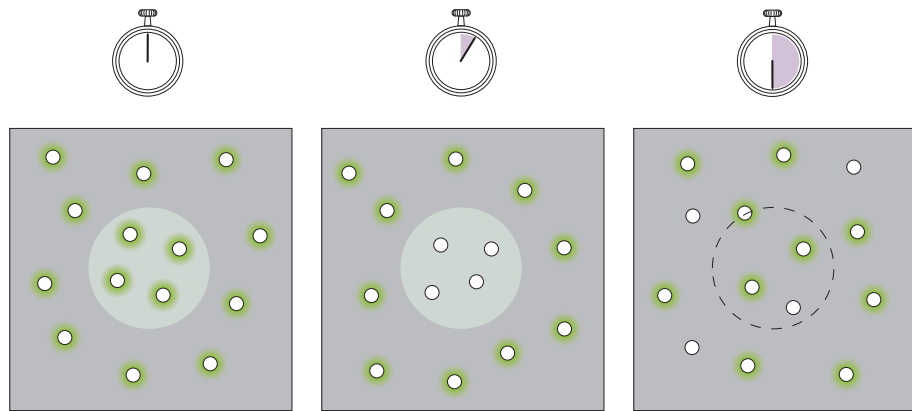


Figure 5.31: Schematic of the FRAP experiment. A particular region of the cell is photobleached, effectively destroying the fluorescent molecules in that region (as shown in the second frame). Recovery of fluorescence in the photobleached region results from fluorescent molecules from elsewhere in the sample diffusing into the photobleached region.

increasing fluorescence over time as new molecules from outside the bleached region diffuse into that region in a process known as recovery. Section 5.5.2 (p. 315) explores the mathematical foundations of this technique and describes the insights it provides.

A more direct technique for monitoring diffusive dynamics is through explicit particle tracking in which individual trajectories are monitored. This technique is as old as the subject of Brownian motion itself, and was used as the basis of measuring atomic dimensions (and Avogadro's number) in the classic experiments of Perrin (1990) as shown in Figure 5.2 (p. 279). The notion of trajectory mapping is of widespread interest and has been used on problems ranging from the motions of bacteria to the wandering of individual proteins along DNA. In this case, the idea usually involves video microscopy (see Figure ??, p. ?? for an example) in which images of the moving species of interest are captured at a fixed interval and the corresponding trajectory is constructed. In the bacterial setting, the nature of the trajectories of motile cells reveals that they have preferences for moving in the direction of certain nutrients, the phenomenon of chemotaxis to be taken up in detail in Chapter 19.

Another technique of great utility for probing diffusive dynamics within cells is FCS. The idea of FCS is to measure the fluorescence intensity in a small region of the cell as a function of time as shown in Figure 5.33. The intensity fluctuates as the fluorescent molecules enter and leave the region under observation. By analyzing the temporal fluctuations of the intensity through the use of time-dependent correlation functions, the diffusion constant and other characteristics of the molecular motion can be uncovered.

JT: Make a big deal out of correlation functions

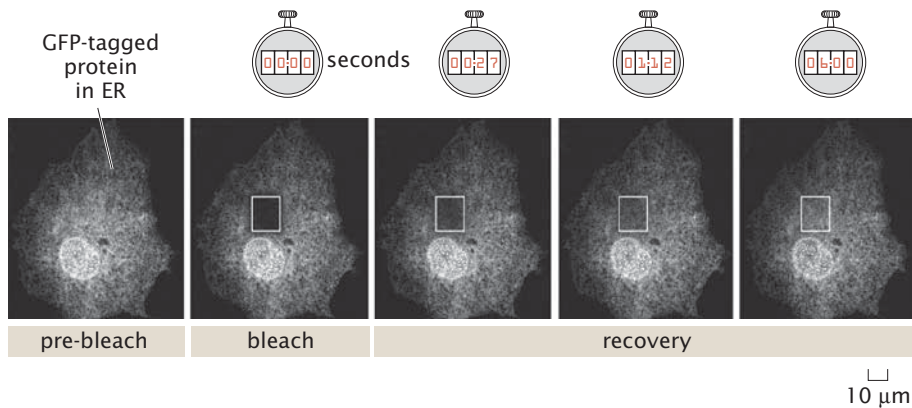


Figure 5.32: FRAP experiment showing recovery of a GFP-labeled protein confined to the membrane of the endoplasmic reticulum. The boxed region is photobleached at time instant,  $t = 0$ . In subsequent frames, fluorescent molecules from elsewhere in the cell diffuse into the bleached region. (Adapted from J. Ellenberg et al., *J. Cell Biol.* 138:1193, 1997.)

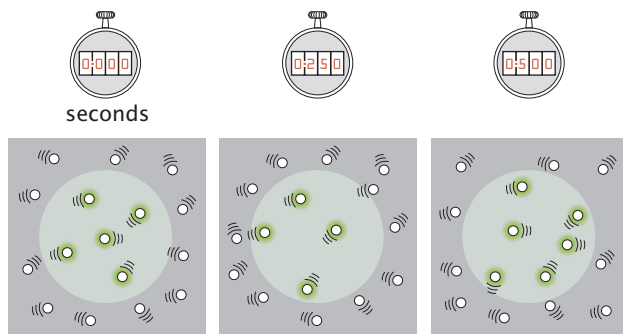


Figure 5.33: Schematic of the FCS technique. The intensity of fluorescent light coming from illuminated molecules is measured as a function of time. The intensity varies in time as a result of molecules diffusing in and out of the observation region, shown in pale green.

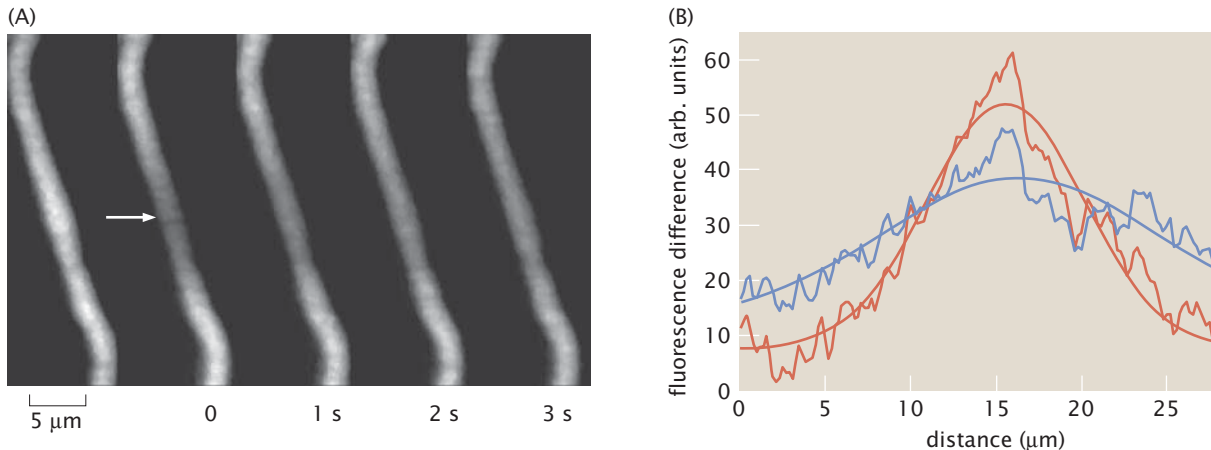


Figure 5.34: FRAP data from a bacterium labeled with GFP. (A) The images show an elongated bacterium with the pre-bleach image on the left and subsequent images taken at different times (reported in seconds) after photobleaching. The arrow shows the photobleached region. (B) The curves show the difference in the intensity profiles before and after photobleaching, along the long axis of the bacterium. The red curve is measured right after photobleaching while the blue curve was obtained from an image acquired 4 s later. (Adapted from C. W. Mullineaux et al., *J. Bacteriol.* 188:3442, 2006.)

The diffusive behavior of a molecule in the environment of a cell depends upon the physical structure of the molecule itself and also on the structure of its environment as well as its interactions with other molecules. In Chapter ?? we will explore some specific cases of how information can be gleaned about cell structure by examining deviations from the diffusive behavior expected in dilute solutions. Here we start with a simple experimental case examining the motion of tracer molecules such as GFP within living cells where the tracer molecule does not form any specific binding reactions with cellular constituents. An example of this sort of experiment is shown in Figure 5.34 for an experiment in which elongated *E. coli* cells are photobleached and the resulting fluorescence intensity is measured over time.

To calculate the expected time evolution of GFP following photobleaching, consider a one-dimensional *E. coli* such as might be found in the gut of a spherical cow (see Figure 21.2 on p. 1738). We leave the more realistic two-dimensional problem to the end of the chapter, though we note that the key features of the problem are already revealed in the one-dimensional case. We consider a one-dimensional model of a FRAP experiment. The fluorescent molecules diffuse in a box of length  $2L$ , which for convenience we place between  $-L$  and  $L$  along the  $x$ -axis. The initial concentration is equal to  $c_0$  on the intervals  $-L < x < -a$  and  $a < x < L$  and is zero on the interval  $-a < x < a$  as is shown in Figure 5.35. In other words, we imagine that we start with a uniform concentration  $c_0$  of fluo-

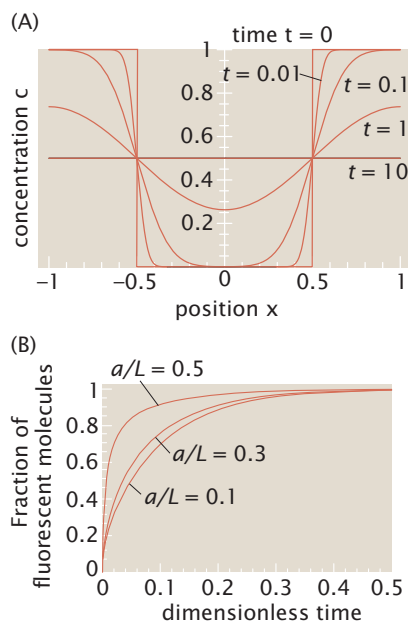


Figure 5.35: One-dimensional model of FRAP. (A) Concentration profile for different times after photobleaching. The bleached region is half the size of the confining region,  $2L$ . (B) Fluorescence recovery as a function of time for different sizes of bleached regions. Recovery is fastest when the bleached region is half the size of the confining region. In both graphs, time is measured in units of  $L^2/D$  and length in units of  $L$ .

rescent molecules in the width- $2L$  box and then we photobleach all the molecules in a smaller box of size  $2a$  by exposing them to intense laser light. If we were to look under a microscope, we would observe the recovery of fluorescence as the nonbleached molecules made their way into the box of size  $2a$ . Based on the speed of fluorescence recovery, the diffusion constant of the fluorescent molecules can be measured.

We can use the simple one-dimensional model to gain quantitative insight into the recovery process. To compute the recovery curves, we first solve the diffusion equation

$$\frac{\partial c}{\partial t} = D \frac{\partial^2 c}{\partial x^2} \quad (5.35)$$

for the concentration of fluorescent molecules  $c(x, t)$ , with the initial concentration after photobleaching given by

$$c(x, 0) = \begin{cases} c_0 & \text{for } -L < x < -a, \\ 0 & \text{for } -a < x < a, \\ c_0 & \text{for } a < x < L. \end{cases} \quad (5.36)$$

We also impose the boundary condition  $\partial c / \partial x = 0$  for  $x = \pm L$ , which says that the flux of fluorescent molecules vanishes at the boundaries of the one-dimensional cell (no material flows in or out). This mimics the real-life situation with fluorescent proteins confined to the volume of the cell, to the cell membrane, or to some other subcellular structure.

To solve the diffusion equation with the prescribed initial and boundary conditions, we begin by expanding the concentration profile  $c(x, t)$  in terms of cosine functions (introduced in The Math Behind the Models on p. 322),

$$c(x, t) = A_0(t) + \sum_{n=1}^{\infty} A_n(t) \cos\left(\frac{x}{L}n\pi\right). \quad (5.37)$$

This expansion guarantees that the boundary conditions are met, namely each of the functions  $A_n(t) \cos(xn\pi/L)$  has vanishing first derivatives at  $x = \pm L$ . Furthermore, since the initial concentration profile takes the same values for positive and negative  $x$ , it is readily expanded in cosine functions. The solution of the diffusion equation now boils down to finding the functions  $A_n(t)$  such that both Equation 5.35 and the initial condition, Equation 5.36, are satisfied.

To proceed, we substitute the series expansion of  $c(x, t)$  into the diffusion equation. This yields

$$\frac{\partial A_0}{\partial t} + \sum_{n=1}^{\infty} \frac{\partial A_n}{\partial t} \cos\left(\frac{x}{L}n\pi\right) = D \sum_{n=1}^{\infty} \left[ -A_n(t) \frac{n^2\pi^2}{L^2} \right] \cos\left(\frac{x}{L}n\pi\right), \quad (5.38)$$

which, due to the orthogonality property of the cosine functions for different  $n$

(see Equation 5.42 below), turns into a set of independent differential equations,

$$\begin{aligned}\frac{\partial A_0}{\partial t} &= 0, \\ \frac{\partial A_n}{\partial t} &= -\frac{Dn^2\pi^2}{L^2}A_n(t) \quad (n \geq 1).\end{aligned}\tag{5.39}$$

The solution to each one of these (infinite in number) equations is an exponential function

$$A_n(t) = A_n(0)e^{-(Dn^2\pi^2/L^2)t},\tag{5.40}$$

which when substituted into Equation 5.37 gives

$$c(x, t) = A_0(0) + \sum_{n=1}^{\infty} A_n(0)e^{-(Dn^2\pi^2/L^2)t} \cos\left(\frac{x}{L}n\pi\right).\tag{5.41}$$

The final piece of the puzzle is the determination of the constants  $A_n(0)$ .

To compute the initial amplitudes of the cosine functions, we once again resort to the orthogonality property of these functions,

$$\int_{-L}^L \cos\left(\frac{x}{L}n\pi\right) \cos\left(\frac{x}{L}m\pi\right) dx = L\delta_{n,m}.\tag{5.42}$$

In particular, we multiply both sides of Equation 5.41 by  $\cos(n\pi x/L)$  for different values of  $n$ , and then integrate over  $x$ , which provides us with the equations

$$\begin{aligned}A_0(0) &= \frac{1}{2L} \int_{-L}^L c(x, 0) dx, \\ A_n(0) &= \frac{1}{L} \int_{-L}^L c(x, 0) \cos\left(\frac{x}{L}n\pi\right) dx \quad (n \geq 1)\end{aligned}\tag{5.43}$$

for the initial amplitudes. Substituting the initial concentration profile,  $c(x, 0)$ , into these equations, and performing the integrals, we arrive at

$$\begin{aligned}A_0(0) &= c_0 \frac{L-a}{L}, \\ A_n(0) &= -2c_0 \frac{\sin(n\pi a/L)}{n\pi} \quad (n \geq 1).\end{aligned}\tag{5.44}$$

Putting these results back into the derived formula for  $c(x, t)$ , Equation 5.41 gives us the solution for the concentration profile as a function of time,

$$c(x, t) = c_0 \left[ 1 - \frac{a}{L} - \sum_{n=1}^{\infty} \frac{2\sin(n\pi a/L)}{n\pi} e^{-(Dn^2\pi^2/L^2)t} \cos\left(\frac{x}{L}n\pi\right) \right],\tag{5.45}$$

which is plotted as a function of  $x$  for different times (and setting  $a = L/2$ ) in Figure 5.35(A). Note that at long times, such that  $t$  is much greater than

$L^2/D$ , which is the diffusion time for a box of length  $L$ , the concentration profile tends to a constant value equal to  $c_\infty = c_0(1 - a/L)$ . This can be understood in a very simple way. Namely, at long times, we expect diffusion to make the concentration profile uniform over the  $2L$  interval. Then, the fact that the number of fluorescent molecules does not change in time leads to the equation

$$c_\infty(2L) = c_0[2(L - a)], \quad (5.46)$$

which gives the computed value of the concentration at long times.

Given the concentration profile as a function of time, we are now in the position to compute a FRAP recovery curve within our simple one-dimensional model. We ask how many fluorescent molecules there are in the bleached region as a function of time. In our simple model, the bleached region is a box that spans from  $-a$  to  $a$  on the  $x$ -axis. We already know that at  $t = 0$ , the number of fluorescent molecules in the bleached region is  $N_f = 0$ , while at times much longer than the diffusion time, this number tends to  $c_\infty(2a)$ . For intermediate times, we need to compute

$$N_f(t) = \int_{-a}^a c(x, t) dx. \quad (5.47)$$

Substituting our result for the concentration profile given in Equation 5.45 into the integral leads to an expression for the recovery curve,

$$\begin{aligned} N_f(t) &= 2c_0a \left(1 - \frac{a}{L}\right) \\ &\times \left[1 - \frac{1}{(a/L)(1-a/L)} \sum_{n=1}^{\infty} \frac{2}{n^2\pi^2} \sin^2\left(\frac{n\pi a}{L}\right) e^{-(Dn^2\pi^2/L^2)t}\right]. \end{aligned} \quad (5.48)$$

Note that at very long times,  $N_f$  approaches  $c_\infty(2a) = 2c_0a(1 - a/L)$ , as expected.

In Figure 5.35(B), we plot a FRAP recovery curve normalized by  $2c_0a(1 - a/L)$ , the total number of fluorescent molecules in the bleached region in the long-time limit. The model makes an interesting prediction that the recovery is fastest when the size of the bleached region is equal to half the size of the confining region. Furthermore, the recovery curves are identical for bleached regions of fractional size  $a/L$  and  $1 - a/L$ , which follows directly from Equation 5.48. In particular, the right-hand side of this equation is invariant under the exchange  $a/L \leftrightarrow 1 - a/L$ .

#### The Math Behind the Models: Expanding in Sines and Cosines

Throughout the book, we are often invited to consider functions that are defined on the interval between 0 and  $L$ . A useful property of such functions that we employ over and over again is that they can be expanded into a Fourier series given by

$$f(x) = \frac{a_0}{2} + \sum_{n=1}^{\infty} \left[ a_n \cos\left(\frac{2\pi n}{L}x\right) + b_n \sin\left(\frac{2\pi n}{L}x\right) \right]. \quad (5.49)$$

Here  $a_n$  and  $b_n$  are Fourier coefficients, numbers that need to be computed for a given function  $f$  and that encode the special features of the function of interest. The above equality is true for all points on the interval, with the possible exception of  $x = 0$  and  $x = L$ . Since all the functions appearing in the sum on the right-hand side take on the same value at 0 and  $L$ , we would have to conclude that  $f(0) = f(L)$  is also true. If this is not the case, it can be shown that the Fourier series representation of  $f(x)$  takes on the value  $[f(0) + f(L)]/2$  at the boundaries of the interval.

Computing the Fourier coefficients relies on the orthogonality property of sine and cosine functions. In particular, the integral of the product of two such functions is nonzero only in the case in which both functions are sines, or both are cosines, and they have the same period; the period of  $\sin(2\pi n/L)$  is  $L/n$ . We can restate this mathematically as

$$\begin{aligned} \int_0^L \sin\left(\frac{2\pi n}{L}x\right) \cos\left(\frac{2\pi m}{L}x\right) dx &= 0, \\ \int_0^L \sin\left(\frac{2\pi n}{L}x\right) \sin\left(\frac{2\pi m}{L}x\right) dx &= \delta_{n,m} \frac{L}{2}, \\ \int_0^L \cos\left(\frac{2\pi n}{L}x\right) \cos\left(\frac{2\pi m}{L}x\right) dx &= \delta_{n,m} \frac{L}{2}, \end{aligned} \quad (5.50)$$

where the Kronecker symbol  $\delta_{n,m}$  is 1 for  $n = m$  and zero otherwise. With these identities in hand, we can compute the Fourier coefficients of the function  $f(x)$  by multiplying it with sines and cosines with different periods, and integrating over the interval between 0 and  $L$ . Looking at the right-hand side of Equation 5.49 and taking into account the orthogonality identities above, we see that the only surviving term on the right-hand side is the sine or cosine term with the same period. Therefore, we have the following identities:

$$\begin{aligned} \int_0^L f(x) dx &= \frac{a_0}{2} L, \\ \int_0^L f(x) \cos\left(\frac{2\pi n}{L}x\right) dx &= a_n \frac{L}{2}, \\ \int_0^L f(x) \sin\left(\frac{2\pi n}{L}x\right) dx &= b_n \frac{L}{2} \end{aligned} \quad (5.51)$$

from which we can compute the Fourier coefficients

$$\begin{aligned} a_0 &= \frac{2}{L} \int_0^L f(x) dx, \\ a_n &= \frac{2}{L} \int_0^L f(x) \cos\left(\frac{2\pi n}{L}x\right) dx, \\ b_n &= \frac{2}{L} \int_0^L f(x) \sin\left(\frac{2\pi n}{L}x\right) dx. \end{aligned} \quad (5.52)$$

To illustrate the procedure of expanding a function into a Fourier series, consider the simple example given by the function  $f(x)$  that is equal to 1 for  $0 < x < L/2$  and equal to zero for  $L/2 < x < L$  (that is, a square wave). Fourier coefficients are computed using Equation 5.52, and we find  $a_0 = 1$ ,  $a_n = 0$  for any other value of  $n$ ,  $b_n = 0$  for  $n$  even, and  $b_n = 2/(\pi n)$  for  $n$  odd. How the function  $f(x)$  emerges from the Fourier series as more and more terms are kept in the sum is shown in Figure 5.36.

## 5.6 The Chemical Master Equation Approach

In this chapter, we celebrate the many different ways to view the phenomenon of diffusion. As shown in Figure 5.39 these different treatments can use different “kinematic” descriptions, electing either to focus on the number of particles, the concentration or even the probability of finding a particle at a given position  $x$ . Having thus far carried out the treatments involving individual walkers using coin flips and random walkers as well as the concentration perspective culminating in the diffusion equation, we now turn to the consideration of a probabilistic description of diffusion, introducing methods that we will return to over and over throughout the book and which we urge the reader to embrace for their own work as well.

The diffusion equation derived in the previous section can be obtained completely differently from a microscopic perspective. The key idea in this case is to consider the motions of individual diffusing molecules (or particles) and to sum over all of the possible microscopic trajectories of the system. The overall macroscopic response emerges as the average over all of these underlying microtrajectories. An example of one particular microtrajectory for a one-dimensional diffusion problem is shown in Figure 5.37.

Particles or fluorescently labeled molecules observed in a microscope are seen to undergo random jiggling, with each particle suffering a different trajectory. We now place these random trajectories front and center and elaborate on a quantitative treatment of diffusion that parallels the states-and-weights approach to computing equilibrium probabilities that will be used throughout the book. In later chapters, we will make use of this “trajectories-and-weights” approach to random dynamics of diffusing particles, molecular motors, polymerization motors, etc. Here we illustrate this procedure on the simple diffusion process. The key idea is to describe a random trajectory by the probability

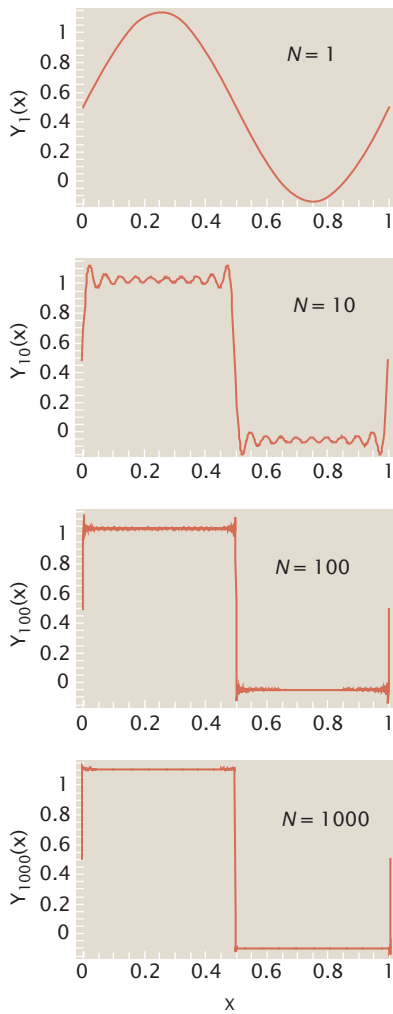


Figure 5.36: Fourier series representation of a square wave. Different graphs correspond to the Fourier series representation of the square wave function where the first  $N$  terms have been retained in the sum on the right-hand side of Equation 5.49.

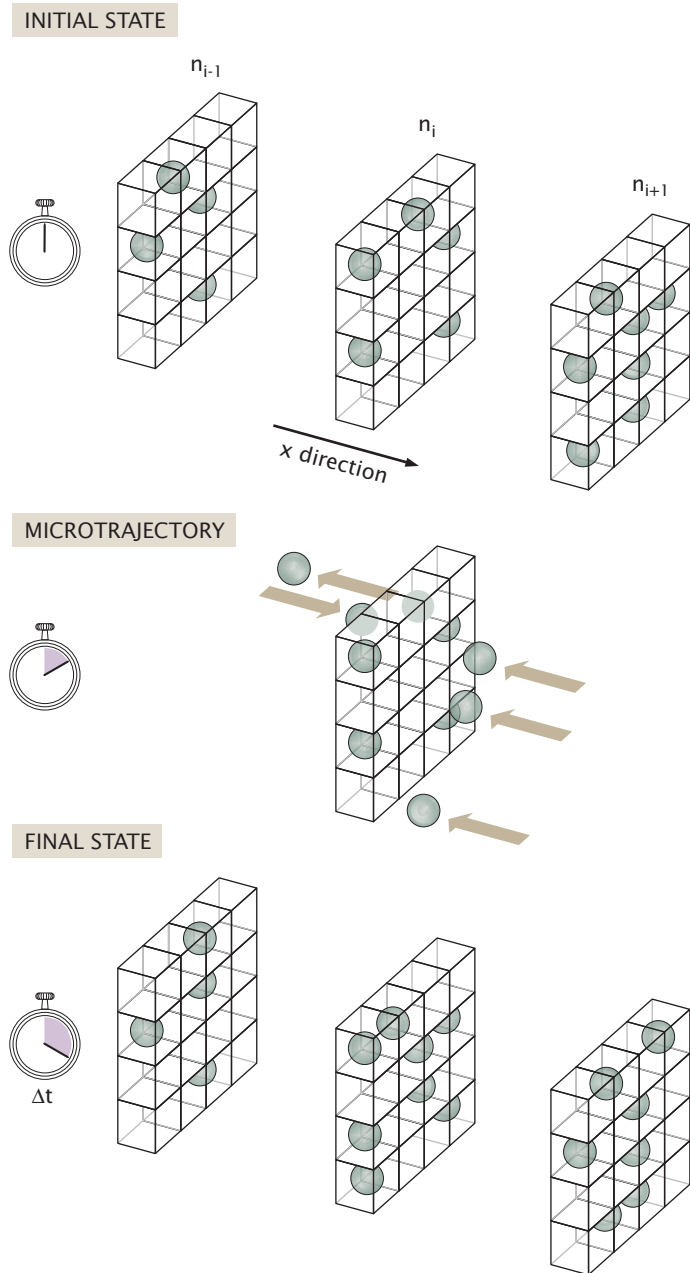


Figure 5.37: Schematic of a particular microscopic trajectory that could occur during a time step  $\Delta t$  for a one-dimensional diffusive profile. Space is discretized into a set of planes and a given microtrajectory results when some particular subset of the molecules jump towards the central plane.

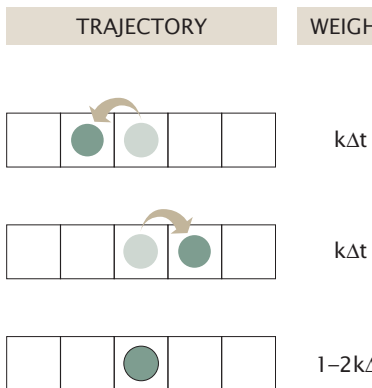


Figure 5.38: Trajectories and weights for simple diffusion. A given diffusing particle can do one of three things at every time step: jump left, jump right, or stay put. Each of these microtrajectories has an associated statistical weight.

density for finding a particle at a particular position at a given instant in time,  $p(\mathbf{x}, t)$ . In particular, the probability of finding the particle in a box of width  $\Delta x$  centered at point  $x$  at time  $t$  is given by  $p(x, t)\Delta x$ . To simplify the math, we specialize to one-dimensional motion, and discretize space and time. In this case, particle trajectories can be compactly denoted as long lists of integers that specify the position of the particle in units of  $a$  at different instants of time, measured in units of  $\Delta t$ . To derive the governing equation for the probability  $p(x, t)$ , we only have to specify the weights of all realizations of microtrajectories that can occur over time  $\Delta t$ .

Microtrajectories and their corresponding weights are shown in Figure 5.38. The diffusing particle, over time  $\Delta t$ , stays put, or jumps to the left or right a distance  $a$ , where we imagine that the particles can only occupy lattice sites on a lattice with spacing  $a$ . The probability of making a jump in either direction is  $k\Delta t$ , while the probability of staying put is  $1 - 2k\Delta t$ , insuring that the probabilities for all three possible outcomes add up to 1. We can use this model to compute a number of quantities associated with the particle displacement over time  $t$ . In time  $t$ , the particle makes a total of  $N = t/\Delta t$  steps, each accompanied by a displacement  $\Delta x_i$ ,  $i = 1, 2, \dots, N$ . The total displacement,  $\Delta x_{\text{tot}} = \Delta x_1 + \Delta x_2 + \dots + \Delta x_N$ , is a sum of independent identically distributed random variables. Therefore, as shown in The Tricks Behind the Math at the end of this section, the mean and the variance of  $\Delta x_{\text{tot}}$  are simply  $N$  times the mean and variance of  $\Delta x$ , the displacement for one time step. These are readily calculated from Figure 5.38 by summing over microtrajectories. We obtain the mean by summing over the three microtrajectories that can occur during a given time step as

$$\langle \Delta x \rangle = a \times k\Delta t + (-a) \times k\Delta t + (0) \times (1 - 2k\Delta t) = 0. \quad (5.53)$$

We can compute the variance as the average of the square of displacement once again by summing over all of the eventualities at a given instant as

$$\langle \Delta x^2 \rangle = a^2 \times k\Delta t + (-a)^2 \times k\Delta t + (0)^2 \times (1 - 2k\Delta t) = 2a^2 k\Delta t. \quad (5.54)$$

The variance of the total displacement is  $N = t/\Delta t$  times greater, resulting in

$$\langle \Delta x_{\text{tot}}^2 \rangle = 2(a^2 k) t, \quad (5.55)$$

which is the result for diffusive spreading if we identify  $a^2 k$  with the diffusion constant  $D$ .

**The Tricks Behind the Math: Averaging Sums of Random Variables**

Independent identically distributed random variables  $\sigma_1, \sigma_2, \dots, \sigma_N$  all have the same probability distribution,  $P(\sigma)$ , and their joint probability distribution factorizes,

$$P_{\text{joint}}(\sigma_1, \sigma_2, \dots, \sigma_N) = P(\sigma_1) \times P(\sigma_2) \times \dots \times P(\sigma_N). \quad (5.56)$$

The factorization property simply means that the probability that one of the random variables takes on a particular value is independent of all the other random variables in the bunch. If the variables  $\sigma_i$  take on two values, say 1 and 0, this mathematical construct could be used, for example, to describe  $N$  noninteracting ion channels, with 0 and 1 corresponding to a channel being closed or open. Beyond this example, there are many more that we will encounter, so we take a brief interlude here to derive two useful identities for the sum of independent identically distributed random variables.

We begin by showing that the average value of the sum,  $\sigma_1 + \sigma_2 + \dots + \sigma_N$ , is equal to  $N$  times the average of one of the random variables (since they are identical, it doesn't matter which one we choose). We start by writing the average of the sum using the joint probability distribution,

$$\left\langle \sum_{i=1}^N \sigma_i \right\rangle = \sum_{\sigma_1} \sum_{\sigma_2} \dots \sum_{\sigma_N} \left[ \sum_{i=1}^N \sigma_i P_{\text{joint}}(\sigma_1, \sigma_2, \dots, \sigma_N) \right]. \quad (5.57)$$

Then, we make use of the factorization property given in Equation 5.56, and the above equation can be written as

$$\begin{aligned} \left\langle \sum_{i=1}^N \sigma_i \right\rangle &= \sum_{\sigma_1} \sigma_1 P(\sigma_1) \sum_{\sigma_2} P(\sigma_2) \dots \sum_{\sigma_N} P(\sigma_N) \\ &\quad + \sum_{\sigma_1} P(\sigma_1) \sum_{\sigma_2} \sigma_2 P(\sigma_2) \dots \sum_{\sigma_N} P(\sigma_N) \\ &\quad + \dots \sum_{\sigma_1} P(\sigma_1) \sum_{\sigma_2} P(\sigma_2) \dots \sum_{\sigma_N} \sigma_N P(\sigma_N). \end{aligned} \quad (5.58)$$

Finally, using the fact that all the probabilities must add up to 1 ( $\sum_{\sigma} P(\sigma) = 1$ ) and the fact that all the random variables are identical, we arrive at the

desired result, namely,

$$\left\langle \sum_{i=1}^N \sigma_i \right\rangle = N \sum_{\sigma} \sigma P(\sigma) = N \langle \sigma \rangle. \quad (5.59)$$

Next, we compute the variance of the sum of  $N$  independent identically distributed random variables. The variance is the average of the square of the difference between the random variable and its mean,

$$\text{var} \left( \sum_{i=1}^N \sigma_i \right) = \left\langle \left( \sum_{i=1}^N \sigma_i - \left\langle \sum_{i=1}^N \sigma_i \right\rangle \right)^2 \right\rangle. \quad (5.60)$$

Using the average computed above, and expanding the square, we can simplify the above equation to read

$$\text{var} \left( \sum_{i=1}^N \sigma_i \right) = \left\langle \left( \sum_{i=1}^N \sigma_i \right)^2 \right\rangle - N^2 \langle \sigma \rangle^2. \quad (5.61)$$

Writing the square in the above equation as a product of two equal terms, and being mindful to use different summation variables  $i$  and  $j$  in the two sums, we arrive at

$$\text{var} \left( \sum_{i=1}^N \sigma_i \right) = \left\langle \sum_{i,j=1}^N \sigma_i \sigma_j \right\rangle - N^2 \langle \sigma \rangle^2. \quad (5.62)$$

Now, to compute  $\left\langle \sum_{i,j=1}^N \sigma_i \sigma_j \right\rangle$ , we break up the double sum into two pieces, one with  $N$  terms where  $i = j$ , and the other with the remaining  $N^2 - N$  terms where  $i \neq j$ :

$$\left\langle \sum_{i,j=1}^N \sigma_i \sigma_j \right\rangle = \left\langle \sum_{i=1}^N \sigma_i^2 \right\rangle + \left\langle \sum_{i \neq j; i,j=1}^N \sigma_i \sigma_j \right\rangle. \quad (5.63)$$

Since all the  $\sigma_i$  are independent, for  $i \neq j$  we have

$$\langle \sigma_i \sigma_j \rangle = \langle \sigma_i \rangle \langle \sigma_j \rangle = \langle \sigma \rangle^2.$$

Putting all this back into Equation 5.62, we arrive at the result

$$\begin{aligned} \text{var} \left( \sum_{i=1}^N \sigma_i \right) &= N \langle \sigma^2 \rangle + (N^2 - N) \langle \sigma \rangle^2 - N^2 \langle \sigma \rangle^2 \\ &= N (\langle \sigma^2 \rangle - \langle \sigma \rangle^2) = N \text{ var}(\sigma). \end{aligned} \quad (5.64)$$

In other words, the variance of the sum of  $N$  independent identically distributed random variables is equal to  $N$  times the variance of one.

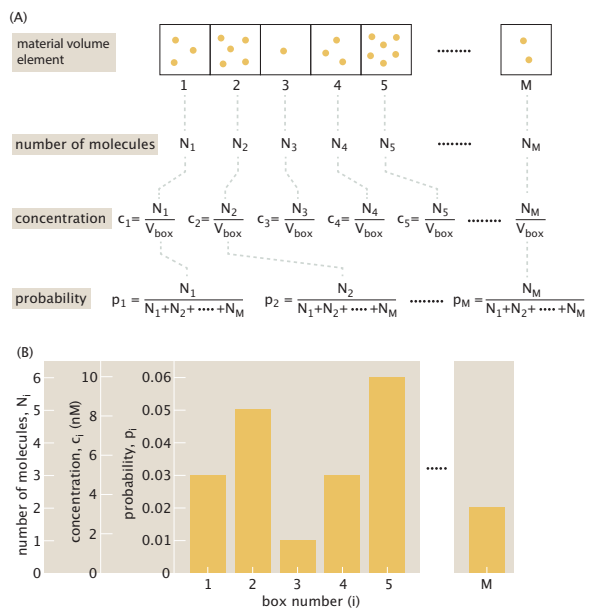


Figure 5.39: Comparing the related concepts of molecular counts, molecular concentrations and molecular probabilities. (A) The cellular milieu containing  $N_{tot}$  molecules is divided into a series of material volume elements of volume  $V_{box}$ . The number of molecules in the  $i^{th}$  box is  $N_i$ . The concentration in the  $i^{th}$  box is  $c_i = N_i/V_{box}$ . The probability of finding a particle in the  $i^{th}$  box is  $p_i = N_i/N_{tot}$ . (B) All of these ways of measuring the number of molecules as a function of position are plotted.

### 5.6.1 Einstein's Approach to the Chemical Master Equation: Diffusion by Summing Over Microtrajectories

Like with many fundamental results, there are multiple ways of deriving the diffusion equation. It is instructive to examine yet another way of deriving this equation, which is another way of summing over all of the microscopic trajectories available to the system at every instant. The approach adopted here is that taken by Einstein in one of his classic 1905 papers. We imagine that time is sliced up into intervals of length  $\Delta t$  and that, at every time step, particles can either jump or stay put. Einstein starts by writing the concentration at position  $x$  and time  $t + \Delta t$  as the following integral:

$$\underbrace{c(x, t + \Delta t)}_{\substack{\text{concentration} \\ \text{at } x \text{ now}}} = \int_{-\infty}^{+\infty} \underbrace{c(x + \Delta, t)}_{\substack{\text{concentration at} \\ x + \Delta \text{ earlier}}} \underbrace{\phi(\Delta)}_{\substack{\text{probability of a} \\ \text{jump of length } \Delta}} d\Delta. \quad (5.65)$$

What this integral says precisely is that to find the concentration at position  $x$  at time  $t + \Delta t$ , we need to sum over all of the possible ways that particles could have gotten there. In particular, at time  $t$ , the particle could have been at position  $x + \Delta$  and then jumped to position  $x$  during the time step. (Note we follow Einstein's notation precisely, so the reader is warned that what Einstein calls  $\Delta$  is our  $\Delta x$  in our earlier derivation of the diffusion equation.) The microtrajectory that we described above can be true for any choice of  $\Delta$ . This means that in order to obtain the concentration at  $x$ , we have to sum over all of the possible jumping events with each one weighted by  $\phi(\Delta)$ , the probability of jumping a distance  $\Delta$ . Effectively, Einstein considers the possibility that particles can jump *any* distance, whereas in our earlier derivation we permitted jumps only of size  $a$ . Einstein makes two further assumptions. First, he posits a symmetry in the jump probabilities of the form

$$\phi(\Delta) = \phi(-\Delta), \quad (5.66)$$

which states that the probability of jumping a certain distance to the right is the same as the probability of jumping that same distance to the left, that is, that there is no bias in the chosen direction. If we included a bias, we would get a driven diffusion equation, which we will encounter in the context of molecular motors. The other key feature of the distribution  $\phi(\Delta)$  is

$$\int_{-\infty}^{+\infty} \phi(\Delta) d\Delta = 1, \quad (5.67)$$

which guarantees that the molecules do *something* at every time step. We now make a familiar refrain by Taylor-expanding both terms appearing in Equation 5.65, which results in

$$c(x, t + \Delta t) \approx c(x, t) + \frac{\partial c}{\partial t} \Delta t \quad (5.68)$$

and

$$c(x + \Delta, t) \approx c(x, t) + \frac{\partial c}{\partial x} \Delta + \frac{1}{2} \frac{\partial^2 c}{\partial x^2} \Delta^2. \quad (5.69)$$

If we substitute these results into Equation 5.65, we find

$$\begin{aligned} c(x, t) + \frac{\partial c}{\partial t} \Delta t &\approx c(x, t) \int_{-\infty}^{+\infty} \phi(\Delta) d\Delta + \frac{\partial c}{\partial x} \int_{-\infty}^{+\infty} \Delta \phi(\Delta) d\Delta \\ &\quad + \frac{1}{2} \frac{\partial^2 c}{\partial x^2} \int_{-\infty}^{+\infty} \Delta^2 \phi(\Delta) d\Delta. \end{aligned} \quad (5.70)$$

The right-hand side of this equation can be examined term by term. The integral in the first term is 1 by Equation 5.67. As a result, we have a term of the form  $c(x, t)$  on both sides of the equation that will cancel out of the final result. The second term is zero because we are integrating an odd function,  $\Delta$ , times an even function,  $\phi(\Delta)$ . If we define the integral in the last term as

$$D \equiv \frac{1}{2\Delta t} \int_{-\infty}^{+\infty} \Delta^2 \phi(\Delta) d\Delta, \quad (5.71)$$

we can write Equation 5.70 as

$$\frac{\partial c}{\partial t} = D \frac{\partial^2 c}{\partial x^2}, \quad (5.72)$$

which is precisely the same result for the one-dimensional diffusion equation that we obtained earlier.

### 5.6.2 Diffusion by Chemical Master Equation

We now turn to the fully general chemical master equation approach that will serve as a recurring theme throughout the book. With tongue in cheek, we sometimes refer to the methods to be described here as “spread the butter” as shown in Figure 5.40 since the key idea is that we are computing the time evolution of the probability, though the total probability remains unchanged in much the same way that as we spread butter, the total amount stays unchanged, though the distribution across the toast varies. This section begins with the probabilistic treatment of diffusion introduced by Einstein, and then turns to the more general formalism to be used throughout the book.

To formulate our thinking, we consider the box centered at position  $x = ia$  as shown in Figure 5.41. Here we shift our emphasis to the quantity  $p(x, t)$  from which we obtain the probability of finding a particle in the box at position  $x = ia$  at time  $t$  as  $p(x, t)\Delta x$ . In a time increment  $\Delta t$ , this probability will change because particles will come into the box of interest from the two adjacent boxes and particles will leave the central box to its two neighbors as shown by the arrows in Figure 5.41.

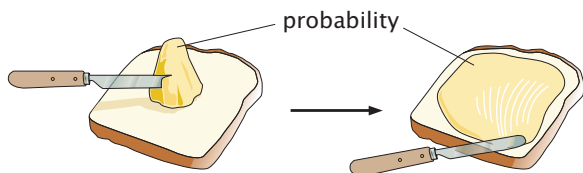


Figure 5.40: Spreading the butter. Describing the temporal evolution of a probability distribution is akin to spreading a given amount of butter onto a piece of toast: the total amount of butter on the toast remains constant.

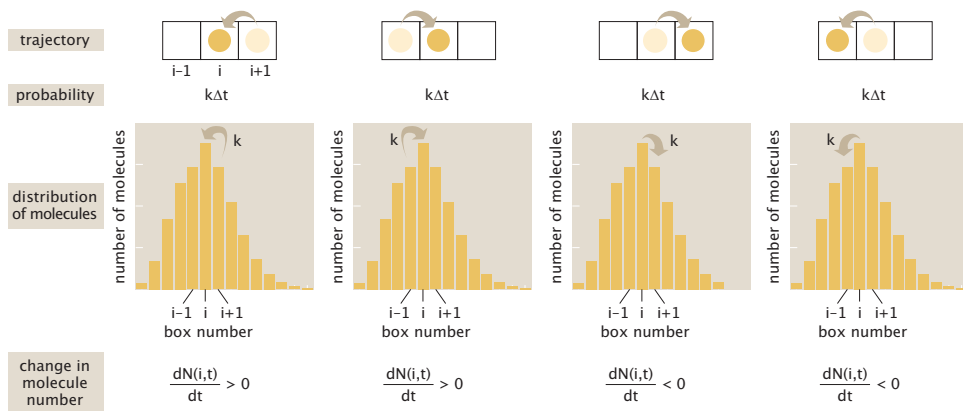


Figure 5.41: Calculating the distribution of molecule diffusing. Protocol for calculating the temporal evolution of the distribution of proteins using the spread-the-butter approach.

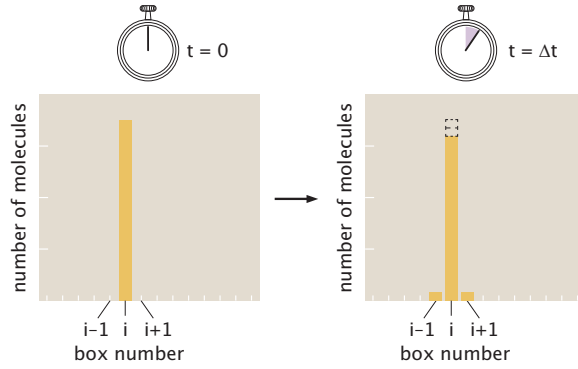


Figure 5.42: Change in the probability distribution for a single time step. In the initial condition shown on the left, all the particles are localized in the box at position  $i$ . Over the time interval  $\Delta t$ , a small number of particles hopped to the right and to the left thus changing the probability distribution.

This intuition for the various changes that can happen in the time increment  $\Delta t$  can be written as

$$p(x, t + \Delta t) = p(x, t) + k\Delta t p(x - a, t) + k\Delta t p(x + a, t) - k\Delta t p(x, t) - k\Delta t p(x, t). \quad (5.73)$$

This amounts to saying that the probability of being found in the box at position  $x$  at time  $t + \Delta t$  is given by the probability of being found in the box at time  $t$ , plus the increase due to jumps into this box from adjacent boxes and minus the loss of probability because particles jump from the box of interest to neighboring boxes. From the perspective of simulating this process on a computer, this is the relevant governing equation and tells us how to “update” the current configuration after a time step  $\Delta t$ . This update is shown explicitly for an extremely simplified situation in Figure 5.42.

It is often analytically convenient to make contact with the differential equation formulation of diffusion. To that end, we can rewrite this as

$$\frac{p(x, t + \Delta t) - p(x, t)}{\Delta t} = ka \left( \frac{(p(x + a, t) - p(x, t))}{a} - \frac{(p(x, t) - p(x - a, t))}{a} \right) \quad (5.74)$$

We can perform another round of simplification by once again recognizing that the quantities in the parentheses in our previous expression are derivatives, thus allowing us to write

$$\frac{p(x, t + \Delta t) - p(x, t)}{\Delta t} = ka^2 \left( \frac{\frac{dp(x+a,t)}{dx} - \frac{dp(x,t)}{dx}}{a} \right) = ka^2 \frac{d^2 p(x, t)}{dx^2} \quad (5.75)$$

We can now rewrite this as

$$\frac{\partial p(x, t)}{\partial t} = (a^2 k) \frac{\partial^2 p(x, t)}{\partial x^2}. \quad (5.76)$$

This is the diffusion equation derived in the previous section from Fick's law, with  $D = a^2 k$ , the same identification we made above.

**Tricks Behind the Math: Spreading the Butter to Solve for Diffusion** Figure 6.50, Figure 5.41

**Computational Exploration: Measuring Diffusion Constants Using FRAP** Earlier in the chapter, we showed how we could solve the diffusion equation analytically using Fourier series for the problem of FRAP of a one-dimensional cell. In this computational exploration, the idea is to perform numerical simulation of that same process using the chemical master equation given in eqn. 5.73. Figure 5.43 gives a sketch of the setup of the problem and specifically Figure 5.43(B) shows how we discretize our hypothetical one-dimensional cell in order to apply eqn. 5.73. The task of this computational exploration is to reproduce the graphs of Figure 5.43(C).

## 5.7 Fun Twists on Diffusion

### 5.7.1 Drunks on a Hill: The Smoluchowski Equation

Thus far, our treatment of diffusion has been based upon those problems in which there are no external forces acting on the particle of interest. On the other hand, there are a number of diffusive processes in which the diffusing species is subjected to a force. For example, we can imagine ion diffusion in the presence of an electric field. In the trajectories-and-weights treatments of diffusion, we assumed that the probabilities of jumping in any of the allowed directions are equal. This is not the case if an external applied force biases the motion of the particle in some particular direction. In this case, we expect the rates to be asymmetrical, since a jump in the direction of the force will be more probable than a jump against the direction of the force. To see the effect of this asymmetry, we can repeat the analysis that led to the derivation of the diffusion equation, but now with the force-induced asymmetry in jump rates.

First we compute the mean and the variance of the particle displacement after time  $t$ . Once again, both the mean and variance of the total displacement are  $N = t/\Delta t$  times greater than the mean and variance of the displacement  $\Delta x$  resulting from a single time step. These statistical quantities are readily computed for a single time step from the trajectories and weights as shown in Figure 5.44, resulting in

$$\begin{aligned}\langle \Delta x \rangle &= a \times k_+ \Delta t + (-a) \times k_- \Delta t = a(k_+ - k_-)\Delta t, \\ \text{var}(\Delta x) &= a^2 \times k_+ \Delta t + (a)^2 \times k_- \Delta t - \langle \Delta x \rangle^2 = a^2(k_+ + k_-)\Delta t\end{aligned}\quad (5.77)$$

where in obtaining the final result for the variance we have dropped the  $\langle \Delta x \rangle^2$  term on account of it being much smaller than the first one; this is because the term that is omitted is quadratic in  $\Delta t$ , or, more precisely, because  $k_{\pm} \Delta t \ll 1$ .

We see that the variance of the displacement is the same as for unbiased diffusion, with the diffusion constant now being given by  $D = (k_+ + k_-)a^2/2$ .